Check for updates

ADVANCED THEORY AND SIMULATIONS
www.advtheorysimul.com

Topology Optimization of Photonic and Phononic Crystals and Metamaterials: A Review

*Weibai Li, Fei Meng, Yafeng Chen, Yang fan Li, and Xiaodong Huang**

This paper presents a comprehensive review of the literature and trends on the design of periodic microstructural composite materials including photonic crystals (PtCs), phononic crystals (PnCs), and metamaterials (MMs) by topology optimization. The properties of these materials rely highly on the constitutive materials and their spatial distributions and the resulting materials may exhibit various special properties, for example, photonic/phononic band gaps, negative permittivity/permeability, negative effective modulus, and negative refraction. Therefore, PtCs, PnCs, and MMs can be viewed as structural materials with periodic unit cells, the design of which is a typical topology optimization problem for desired properties or functionalities. In recent years, a great amount of research has implemented topology optimization for designing these structural materials as well as the associated functional devices. This review summarizes the most recent development in topology optimization of PtCs, PnCs, and MMs and the possible directions for future research are recommended.

1. Introduction

Photonic crystals (PtCs) and phononic crystals (PnCs) are two different classes of artificial medium but have similar structural elements, with some form of spatial periodicity for component material phases, geometry and boundary conditions. The early study of the periodic systems can be traced back to Rayleigh's analysis of the optical property within 1D PtCs in 1887.[1] It was found that such structures have a frequency range of high reflectivity, and this phenomenon is now known as the 1D photonic band gap. Since the concept of PtCs was introduced,[2,3] considerable attention has been attracted in this field. Inspired by the concept of PtCs, the existence of band gaps for the propagation of elastic/acoustic (E/A) waves in the periodic heterogeneous medium was firstly reported by Sigalas and Economou.[4] The term "phononic crystals" was named by Kushwaha in his study of out-of-plane waves in periodic composites.[5] As a result, a variety of opportunities for feasible applications in applied physics and engineering have been created by the success in designing and manufacturing various forms of phononic/photonic band gap (PBG) materials. PtCs have been applied in devices such as optical fiber,[6,7] cavity, and waveguide.[8] For PnCs, vibration isolation,[9] acoustic wave filtering, waveguides and localization[10–12] become realized with notable effects.

The word "metamaterial" first came up in the paper by Smith et al.,[13] which experimentally demonstrated a structured material with a negative refractive index (both permittivity and permeability are negative) in the microwave frequency range. The existence of such materials was first predicted by Veselago[14] in 1968, and it was verified 30 years later, when Pendry et al.,[15] Smith et al.,[13] and Shelby et al.[16] successfully found negative refractive metamaterials constructed by periodic metallic resonant structures. As the counterpart of electromagnetic (EM) MMs, E/A MMs exhibit the possibility to manipulate E/A wave propagation in the subwavelength scale. A vast amount of research has gone into investigating E/A MMs with negative material parameters, e.g. negative bulk/shear modulus and mass density,[17–20] the effective medium theory[19,21] and applications such as near-field amplification[22] and subwavelength imaging.[23]

PtCs, PnCs, and MMs have periodic microstructures in 1D, 2D, or 3D. The unique characteristics of these advanced materials give rise to extraordinary applications, but also raise the question how to distribute constituent materials within a 2D or 3D unit cell so that the resulting materials can achieve the desired properties? Compared with the traditional trial-and-error approach, a systematic and scientific way is to formulate the problem mathematically and then solve it through topology optimization. Topology optimization originated from structural engineering on seeking the distribution of materials within a given domain so that the resulting structure achieves the best or desired performance. Since the pioneering work of Bendsøe and Kikuchi[24] in 1988, various gradient-based topology optimization (GTO) methods, such as solid isotropic material with penalization (SIMP),[25–27] level set (LS),[28–30] and bi-directional evolutionary structural optimization (BESO),[31,32] have been proposed. The non-gradient topology optimization (NGTO) method such as genetic algorithm (GA)[33–35] was also widely used for topology optimization of structures. The computational burden of topology optimization mainly comes from the performance analysis of structures iteratively. NGTO needs a large number

W. Li, Dr. F. Meng, Y. Chen, Dr. Y. F. Li, Prof. X. Huang
Faculty of Science, Engineering and Technology
Swinburne University of Technology
Hawthorn, VIC 3122, Australia
E-mail: xhuang@swin.edu.au

The ORCID identification number(s) for the author(s) of this article can be found under https://doi.org/10.1002/adts.201900017

DOI: 10.1002/adts.201900017

 © 2019 WILEY-VCH Verlag GmbH & Co. KGaA, Weinheim

of structural experiments, and its computational efficiency is a potential issue for topology optimization with a large number of design variables. Topology optimization methods had been detailedly reviewed by many researchers, for example, Rozvany,[36] Sigmund, and Maute.[37] The development of topology optimization methods is of significance and establishes the foundation of their multidisciplinary and multi-physics applications.

In recent years, topology optimization of PtCs, PnCs, and MMs has received tremendous attention. Cadman et al.[38] reviewed the topology optimization of periodic material microstructures for various physical properties including PBG materials. Jensen and Sigmund[39] presented the fundamental procedures behind topology optimization of PtCs for a wide range of photonic functionalities, including slow light, waveguides, filters, pulse modulation devices, non-linear effects, and other related applications. Molesky et al.[40] summarized the development of topology optimization of nano-photonics for the emerging applications, including nonlinear optics, exceptional photonics, nanoscale optics, and metasurfaces. Lu et al.[41] discussed the novel properties of PnCs and acoustic MMs. Hussein et al.[42] overviewed on theoretical studies, computational analysis techniques, and experimental activities of PnCs. Yi and Youn[43] presented a comprehensive survey on topology optimization of PnCs. PtCs, PnCs, and MMs share plenty of similarities in the manipulation of wave propagation, and the objective and constraint functions of topology optimization are formulated on their physical properties and applications. Therefore, this paper will overview their physical properties and applications, and then review the recent development of topology optimization for creating novel designs of PtCs, PnCs, and MMs.

Weibai Li received his master's degree in engineering from Tongji University, China. Currently, he is a Ph.D. student at Swinburne University of Technology, Australia. His research focuses on topology optimization of phononic crystals and metamaterials.

Fei Meng is a research fellow at Swinburne University of Technology, Australia. He received his doctoral degree in 2019 from the same University. His research mainly focuses on topology optimization of photonic crystals and metamaterials.

Xiaodong Huang is professor and ARC future fellow at Swinburne University of Technology, Australia. He was the primary innovator of the gradient-based bidirectional evolutionary structural optimization (BESO) method for designing structures and materials.

2. Photonic Crystals

In contrast to electromagnetic metamaterials, PtCs have an impact on electromagnetic waves with wavelengths comparable to their lattice constants. PtCs consist of two or more dielectric materials and a large contrast between dielectric indices of constituent materials is essential.

2.1. Properties and Application of PtCs

Depending on their microstructures and properties of constituent materials, PtCs have unique optical properties, for example, photonic band gap and negative refraction, which are of high value in manipulating electromagnetic waves.

Photonic band gap defines a range of frequency within which the propagation of electromagnetic waves inside PtCs is totally prohibited. Such a special property is the foundation of many optical applications. Even the simplest form, 1D photonic band gap crystals, can be designed to reflect light incidents from any angle with any polarization, forming an omnidirectional reflector, but in general, the reflection is only for near-normal incidence. For 2D PtCs, there are two possible polarizations: transverse magnetic (TM) and transverse electric (TE) modes. In the TM modes, the electric field is perpendicular to the crystal cross section, while in the TE modes, the magnetic field is perpendicular to the crystal cross section. The overlapped band gaps in both polarizations can be named as a complete band gap. 3D PtCs enable an omnidirectional band gap to prohibit the propagation of electromagnetic waves of any polarization in any direction from any source. The engineering applications of photonic band gaps are highlighted as cavities,[44–52] fibers,[53–63] and waveguides,[64–74] as shown in **Figure 1**.

Negative refraction is a phenomenon where a light beam travels to an interface of two different materials and is refracted to the direction on the same side of the surface as the incident beam. This is contrary to the case of positive index materials. Such property has become of interest because it is the foundation of some special applications like a super lens.[75] For PtCs, negative refraction can be realized based on their exclusive dispersion properties. An all-angle negative refraction (AANR) effect involving 2D PtCs was reported by Luo et al.,[76] in which a negative effective index was unnecessary. The diffraction in PtCs leads to one component of the group velocity propagating the opposite direction of the wave vector **k**, which induces negative refraction as shown in Figure 1r. Investigation of negative refraction in PtCs has also been conducted by many researchers.[77–80] Compared with metamaterials, PtCs can interfere with light, of which wavelengths are comparable to its lattice constant, indicating that they can work at higher frequencies such as optical or infrared regions. Further, typical PtCs composed of dielectric materials have a lower absorption in high-frequency regions.[81] Negative refraction in

© 2019 WILEY-VCH Verlag GmbH & Co. KGaA, Weinheim

25130390, 2019, 7, Downloaded from https://onlinelibrary.wiley.com/doi/10.1002/adts.201900017 by The Librarian, Wiley Online Library on [03/06/2024]. See the Terms and Conditions (https://onlinelibrary.wiley.com/terms-and-conditions) on Wiley Online Library for rules of use; OA articles are governed by the applicable Creative Commons License

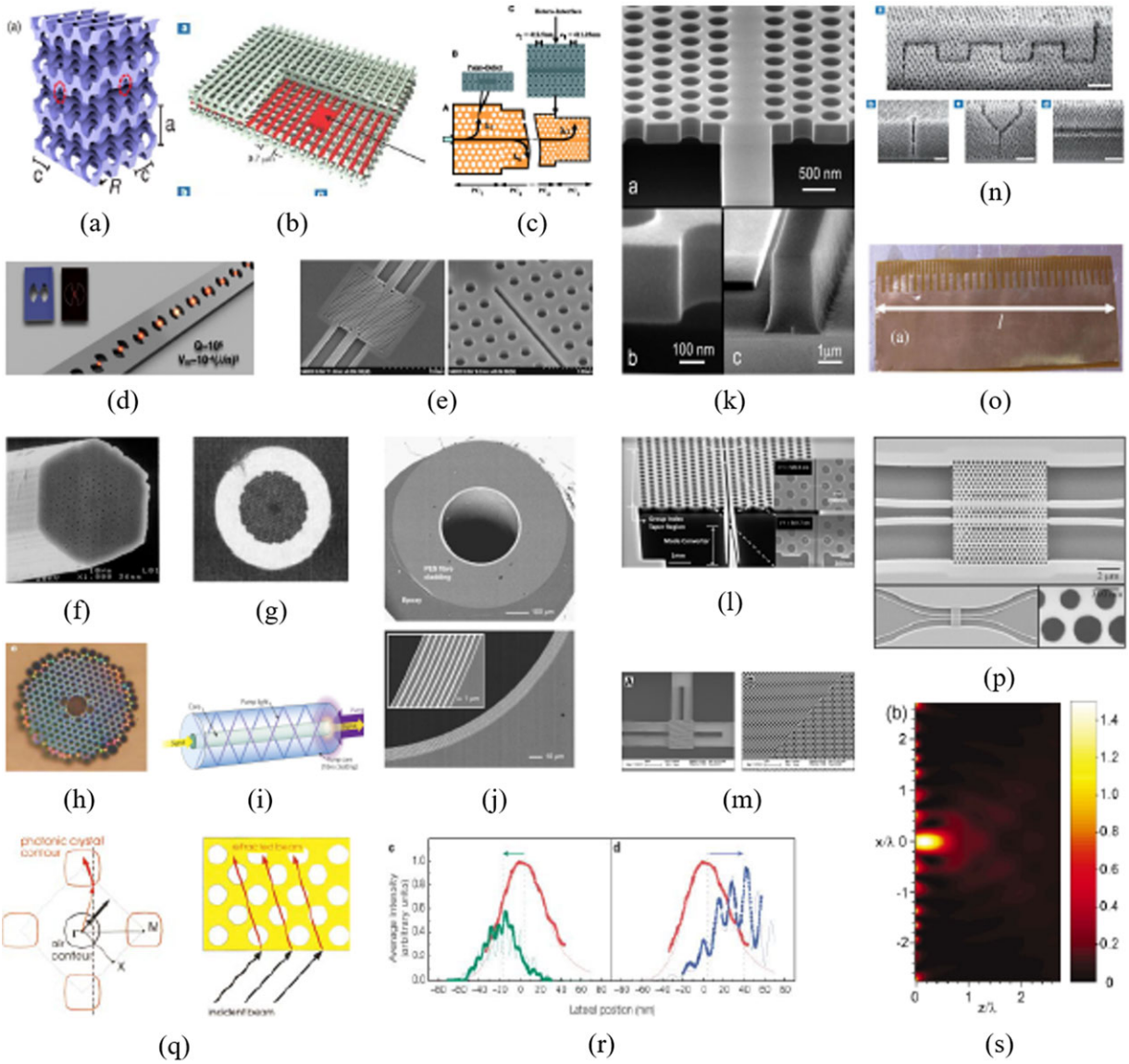

Figure 1. Properties and applications of photonic crystals. Cavities: a) The structure of an inverse woodpile PhC with a point defect; b) spontaneous emission control by self-assembled 3D PtCs; c) a photonic nanostructure device based on in-plane hetero photonic crystals; d) design of photonic crystal cavities for extreme light concentration; e) slotted photonic crystal cavities fabricated in SOI. Fibers: f) a PhC fiber; g) a BlazePhotonic band-gap fiber; h) a PhC fiber; i) schematic of a high-power, double-clad fiber amplifier; j) a hollow core photonic band gap fiber. Waveguides: k) The design and fabrication of a photonic integrated circuit; l) a fabricated PhC slot waveguide device; n) a PhC polarization beam splitter; o) 3D silicon photonic crystals shown as waveguides, Y-shaped splitters, and embedded planar cavities; p) a splitter using a composite periodic grating structure; q) a PhC optical switch. Negative refraction: r) negative-refracted beams constructed from constant-frequency contours and conservation of surface-parallel wavevector; s) negative refraction (left) and positive refraction (right) by PtCs; t) subwavelength imaging in photonic crystals. a) Reproduced under the terms of the Creative Commons Attribution 3.0 License.[51] Copyright 2014, The Authors, published by American Physical Society. b) Reproduced with permission.[49] Copyright 2007, Nature Research. c) Reproduced with permission.[47] Copyright 2003, AAAS. d) Reproduced with permission.[52] Copyright 2016, American Chemical Society. e) Reproduced with permission.[50] Copyright 2011, Elsevier. f) Reproduced with permission.[53] Copyright 1997, Optical Society of America. g) Reproduced with permission.[57] Copyright 2004, American Institute of Physics. h) Reproduced with permission.[55] Copyright 2003, Springer Nature. i) Reproduced with permission.[63] Copyright 2013, Nature Research. j) Reproduced with permission.[7] Copyright 2002, Nature Research. k) Reproduced with permission.[69] Copyright 2003, Optical Society of America. l) Reproduced with permission.[73] Copyright 2011, Optical Society of America. m) Reproduced with permission.[71] Copyright 2006, Optical Society of America. n) Reproduced with permission.[8] Copyright 2007, Nature Research. o) Reproduced with permission.[74] Copyright 2013, American Institute of Physics. p) Reproduced with permission.[72] Copyright 2008, Optical Society of America. q) Reproduced with permission.[76] Copyright 2002, American Institute of Physics. r) Reproduced with permission.[80] Copyright 2008, Nature Research. s) Reproduced with permission.[86] Copyright 2003, American Physical Society.

© 2019 WILEY-VCH Verlag GmbH & Co. KGaA, Weinheim

25130390, 2019, 7, Downloaded from https://onlinelibrary.wiley.com/doi/10.1002/adts.201900017 by The Librarian, Wiley Online Library on [03/06/2024]. See the Terms and Conditions (https://onlinelibrary.wiley.com/terms-and-conditions) on Wiley Online Library for rules of use; OA articles are governed by the applicable Creative Commons License

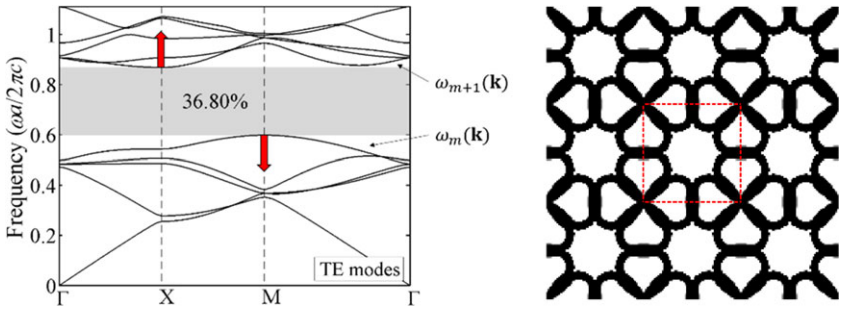

Figure 2. An illustrated band diagram (left) and its corresponding structure of the PtC (right). The band gap occurs between the fifth and sixth bands ($m = 5$).

PtCs can be utilized to achieve a superprism effect[82–84] and perfect imaging.[77,79,85,86]

2.2. Topology Optimization of PtCs

The traditional trial-and-error design approach based on physical intuitions and parametric studies has achieved considerable results for the design of PtCs.[87–90] However, this process is inefficient and time-consuming, and the resulting design may also be far away from an optimum. A systematic way is to formulate the problem with appropriate objective functions and constraints, then solve it by topology optimization techniques.

Topology optimization is an iterative process based on numerical computation. For the analysis of waves propagating in PtCs, as well as PnCs and MMs, several numerical methods, such as finite element method (FEM),[91–95] plane wave expansion (PWE) method,[96,97] and finite-difference time-domain (FDTD) method[98–100] have been established. For more details on numerical methods for the analysis of PtCs, the interested readers can refer to ref. [101].

2.2.1. Photonic Band Gaps

The propagation of electromagnetic waves is entirely prohibited in a particular frequency range called band gap. In practice, a broader band gap range means broader potential applications. It is of great significance for designing PtCs with possible largest band gaps. Topology optimization of photonic band gap crystals, especially in 2D form, has been intensively studied by researchers in the past years.

Cox and Dobson used the density-based topology optimization algorithm to maximize the band gaps in 2D PtCs for both TM[102] and TE[103] modes. Kao et al.[104] and He et al.[105] adopted the level set method to design 2D photonic band gap crystals for both modes. Sigmund and Hougaard[106] developed a two-stage topology optimization, in which the first stage selects the five best topologically different candidates for each band generated by coarse grids. In the second stage, topology optimization aims to maximize the opening band gap of the selected topologies. Men et al. introduced the design of 2D PtCs using semidefinite programming and subspace methods.[107,108] The optimization starts from a series of randomly generated initial designs to obtain the optimized structures, but the success of optimization cannot be guaranteed in achieving desired band gaps. Takezawa and Kitamura[109] proposed the phase field method for 2D photonic crystal design. Compared with the level set approach, this method has the advantage of simplicity without extra re-initializing operations of the domain-representing function. Cheng and Yang[110] considered the photonic band gap maximization problems by using the piecewise constant level set method. The genetic algorithm was also applied by Goh et al.[111] for the design of both 1D and 2D PtCs.

The basic concept of topology optimization methods is the stepwise redistribution of the material within the design domain. Thus, the resulting structure evolves to its optimum. An appropriate objective function is necessary to evaluate the performance of the new structure. For the maximization of a specified band gap of a PtC, the topology optimization problem based on the framework of finite element analysis can be stated as follows:

$$\begin{aligned} &max: f(x_e) = 2\frac{\min\left(\omega_{m+1}(\mathbf{k})\right) - \max\left(\omega_{m+1}(\mathbf{k})\right)}{\min\left(\omega_{m+1}(\mathbf{k})\right) + \max\left(\omega_{m+1}(\mathbf{k})\right)} \\ &s.t.: \nabla\cdot(A\nabla\mathbf{u}) + B\omega^2\mathbf{u} = 0 \\ &V(x_e) - V^* \le 0 \\ &\chi_e = 0 \text{ or } 1 \end{aligned} \tag{1}$$

The objective function is to maximize the gap–midgap ratio between two adjacent bands (illustrated in **Figure 2**). In the governing Maxwell's equations, $A = 1$, $B = \varepsilon(\mathbf{r})c^{-2}$, and $\mathbf{u} = E(\mathbf{k}, \mathbf{r})$ for TM-polarized electromagnetic waves and $A = 1/\varepsilon(\mathbf{r})$, $B = c^{-2}$, and $\mathbf{u} = H(\mathbf{k}, \mathbf{r})$ for TE-polarized electromagnetic waves. E and H are the electric and magnetic fields, respectively. The vector $\mathbf{r} = (x, y, z)$ denotes the coordinates and $\mathbf{k}$ is the wave vector. The design variable, x_e, can be assumed as an elemental parameter to describe the distribution of base materials. For example, a PtC is composed of two dielectric materials with permittivity, ε_1 and $\varepsilon_2(\varepsilon_1 < \varepsilon_2)$. Thus, $x_e = 0$ denotes that the element is full of material 1 and $x_e = 1$ for material 2. However, such a discrete topology optimization problem is difficult to be solved mathematically. In GTO algorithms,[37,112,113] this problem is relaxed to be continuous by $0 \le x_e \le 1$ and the permittivity of each element is properly interpolated.

© 2019 WILEY-VCH Verlag GmbH & Co. KGaA, Weinheim

25130390, 2019, 7, Downloaded from https://onlinelibrary.wiley.com/doi/10.1002/adts.201900017 by The Librarian, Wiley Online Library on [03/06/2024]. See the Terms and Conditions (https://onlinelibrary.wiley.com/terms-and-conditions) on Wiley Online Library for rules of use; OA articles are governed by the applicable Creative Commons License

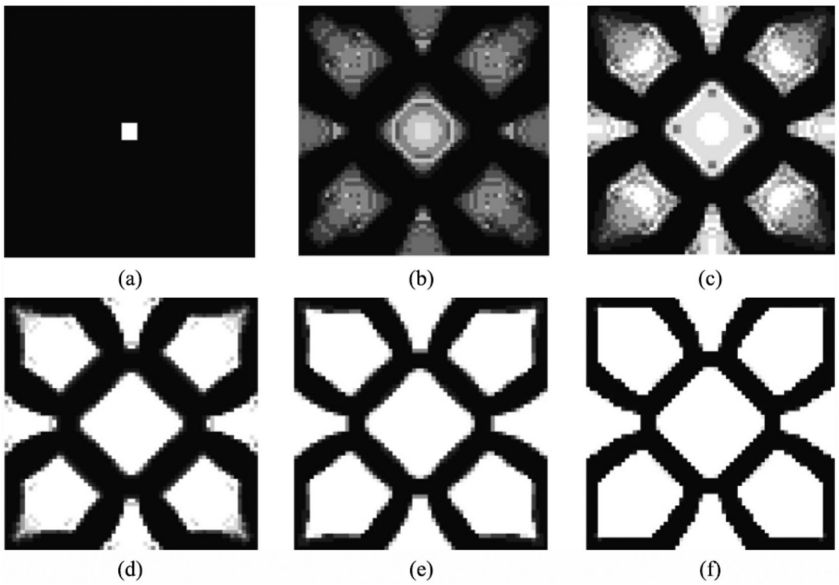

Figure 3. Evolution history of the unit cell for maximizing the seventh band gap of TE mode. a) Initial design. b) Iteration 10. c) Iteration 20. d) Iteration 30. e) Iteration 40. f) Final optimized design. Reproduced with permission.[92] Copyright 2015, Elsevier Inc.

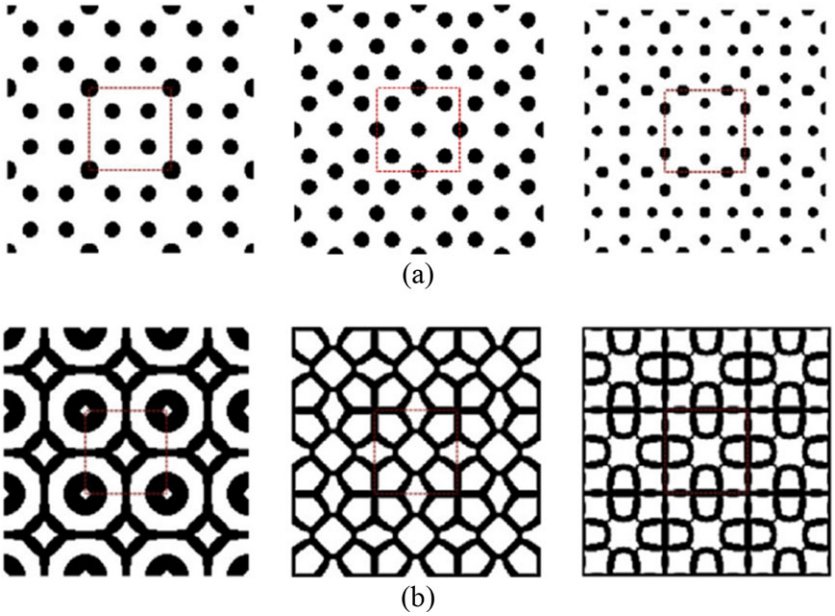

Figure 4. Optimized PtCs. a) 3 × 3 unit cells for TM band gaps, from left to right, the fifth, seventh, and ninth bands. b) 3 × 3 unit cells for TE band gaps, from left to right, the fifth, seventh, and ninth bands. Reproduced with permission.[92] Copyright 2015, Elsevier Inc.

Meng et al.[92] developed an efficient and easy-implement BESO algorithm for 2D photonic band gap structures. The optimization procedure has been developed based on the finite element analysis and sensitivity analysis. Starting from a simple initial design without any band gaps, the dielectric materials are gradually re-distributed within the unit cell so that the resulting photonic crystal possesses a maximum band gap between two specified adjacent bands. **Figure 3** gives an example of the evolution history of topology. Compared with previous results with few band gaps, photonic structures with band gaps from the first to the tenth band for both TE and TM modes were systematically reported. Due to the different formation mechanisms, optimized PtCs for TM and TE modes show different structural features with regard to the distribution of the base material. The material with a high refractive index displays as isolated dielectric "rods" for TM modes (**Figure 4**a), while it constitutes connected "walls" for TE modes (Figure 4b). Later, Meng et al.[114] extended this method for systematically designing 2D symmetric and asymmetric photonic band gap crystals.

Generally, a photonic band gap is called a complete band gap when both the TM and TE waves are prohibited. A complete band gap is of practice since it is independent of the polarization of

© 2019 WILEY-VCH Verlag GmbH & Co. KGaA, Weinheim

25130390, 2019, 7, Downloaded from https://onlinelibrary.wiley.com/doi/10.1002/adts.201900017 by The Librarian, Wiley Online Library on [03/06/2024]. See the Terms and Conditions (https://onlinelibrary.wiley.com/terms-and-conditions) on Wiley Online Library for rules of use; OA articles are governed by the applicable Creative Commons License

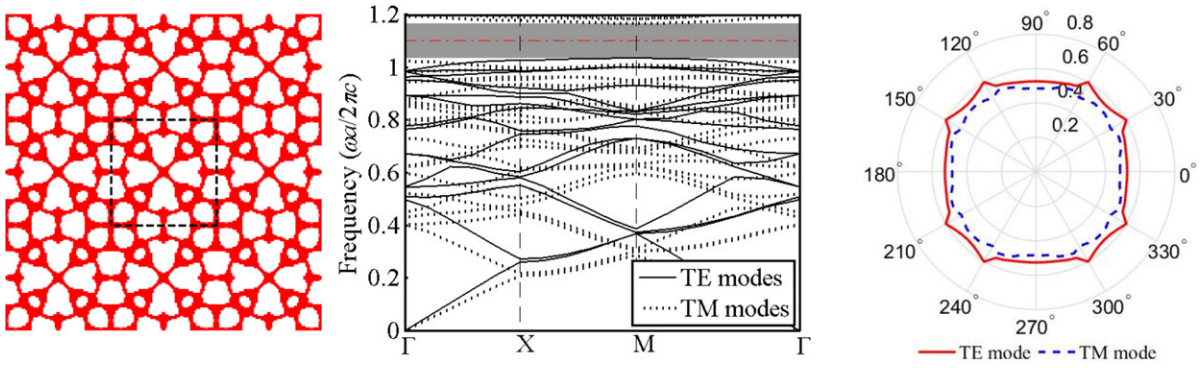

Figure 5. Optimized topology, the corresponding band diagram, and minimum decay contour (minimum imaginary part of wave vector at various angles) for combined TE and TM modes with normalized frequency $\Omega = 1.1$. Reproduced with permission.[119] Copyright 2018, IOP Publishing, Ltd.

light. However, the formation of a TM and TE band gap has different mechanisms.[115] The Mie resonance dominates the TM band gap, while the Bragg scattering occupies the main position in the TE mode, showing different structural features (see Figure 4). Consequently, the opposite structural characteristics make it challenging to achieve PtCs with a complete band gap for both TM and TE modes simultaneously. Shen et al.[116] used a genetic algorithm to find 2D PtCs with large absolute band gap. By combining the geometry projection method with FEM, Wang et al.[117] reported a 2D GaAs/Air PtC with square lattice possessing a large band gap. Meng et al.[118] enlarged the complete band gap from a guess design, which is generated by superposing the optimized topologies of a TE band gap structure and a TM band gap structure. Chen et al.[119] presented a new way to create a complete band gap at any specified frequency through maximizing the minimum imaginary part of wave vectors for both TM and TE modes. The occurrence of a band gap means only evanescent electromagnetic waves are allowed in their designs. The spatial decay of evanescent electromagnetic waves inside the band gap is multi-exponential and dominated by the minimum imaginary part of wave vectors.[81,120] Once the minimum imaginary part of the wave vectors for both modes is larger than zero, the complete photonic band gap at the specified frequency will be automatically opened, as shown in **Figure 5**.

Following the verification of a photonic band gap in periodic dielectric structures,[121] numerous interesting 3D structures have been investigated in the literature, such as woodpile,[122,123] layered structures,[124,125] and spiral structures.[126,127] 3D PtCs have more practical potential than their 2D counterparts due to their ability to manipulate the propagation of electromagnetic waves in all directions. Even so, topology optimization of 3D PtCs is relatively rare, compared with that in 2D form. Men et al.[128] presented the robust topology optimization built on the subspace projection to search the optimized band gaps in simple cubic (SC), body-centered cubic (BCC), and face-centered cubic (FCC) lattices (**Figure 6**a). Their results proved the feasibility of 3D topology optimization for photonic band gaps but produced some 3D structures that had been verified. Meng et al.[129] conducted the systematic topology optimization design for 3D PtCs with maximal omnidirectional band gaps. Considering an asymmetric simple cubic lattice, various novel 3D structures, shown in Figure 6b as examples, with band gaps between any two neighboring bands have been obtained through this method.

2.2.2. PtCs for Negative Refraction

PtCs can take advantage of the exotic dispersion properties mentioned in Section 2.1 and generate AANR even with a positive refractive index. Meng et al.[130] proposed a BESO-based algorithm to design PtCs with a broad frequency range for AANR. The optimization objective was initially established as the maximization of the non-dimensional ratio between the difference of upper limit ω_u and lower limit ω_l of the AANR range and the mean value of them.

$$\max: f(x_e) = \frac{\omega_u - \omega_l}{(\omega_u + \omega_l)/2} \tag{2}$$

Although the objective function in Equation (2) has a clear physical meaning determined by the radius of equi-frequency contour (EFC) curvature, as shown in **Figure 7**a, it is hard to formulate ω_u or ω_l mathematically. To circumvent this problem, a reference point on the first band, with a wave vector adjacent to that of the lower limit ω_l, as shown in Figure 7b, is selected. The lower limit ω_l will be moved toward the reference point as a consequence of maximizing the radius of EFC curvature at the reference point. This process is repeated step by step and the lower limit ω_l will be moved toward the Γ point. Since the upper limit ω_u is determined by the constant light line, the decrease of ω_l is equivalent to the enlargement of the AANR frequency range. Therefore, the objective function of the optimization problem is converted to maximize the radius of EFC curvature at the reference point as follows:

$$\max: R(x_e) = \frac{\left(f_x'^2 + f_y'^2\right)^{3/2}}{f_{xx}'' \cdot f_y'^2 + f_{yy}'' \cdot f_x'^2 - 2 \cdot f_x' \cdot f_y' \cdot f_{xy}''} \times \text{at the reference point} \tag{3}$$

where $f_x' = \frac{\partial \omega}{\partial k_x}$ and $f_y' = \frac{\partial \omega}{\partial k_y}$. f_{xx}'', f_{yy}'', and f_{xy}'' are the second-order partial derivatives. Those derivatives can be calculated by using the finite difference method.

The optimization results are shown in **Figure 8**a–d with AANR sizes 2.56% for the TM mode and 14.08% for the TE mode. In their subsequent work,[131] by analyzing the contour map and dispersion criteria, an easily fabricated "supercircle" structure was

© 2019 WILEY-VCH Verlag GmbH & Co. KGaA, Weinheim

25130390, 2019, 7, Downloaded from https://onlinelibrary.wiley.com/doi/10.1002/adts.201900017 by The Librarian, Wiley Online Library on [03/06/2024]. See the Terms and Conditions (https://onlinelibrary.wiley.com/terms-and-conditions) on Wiley Online Library for rules of use; OA articles are governed by the applicable Creative Commons License

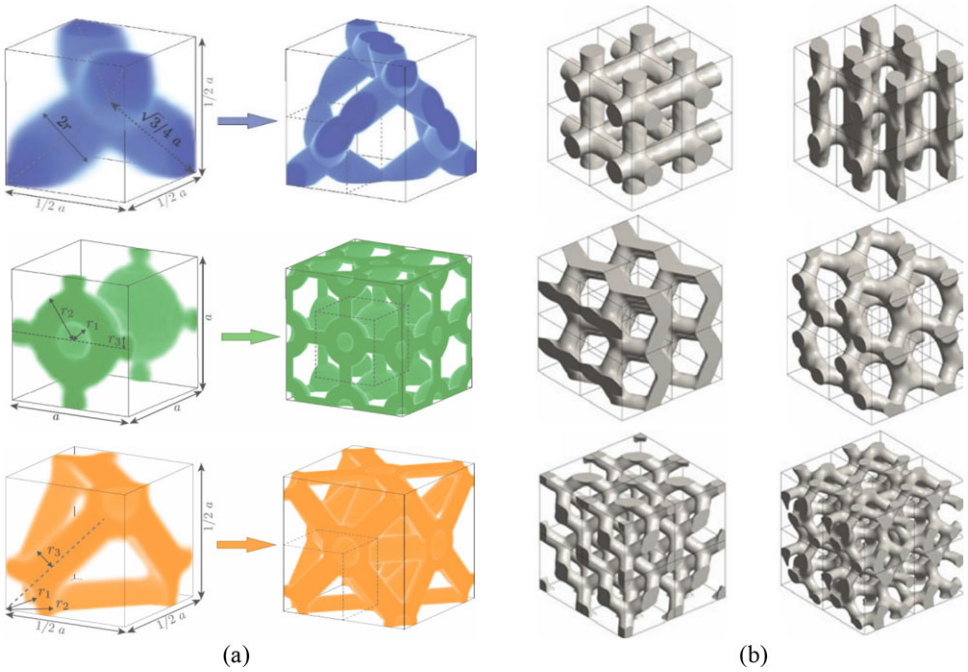

Figure 6. 3D designs of PtCs: a) geometry parameter optimization of PhCs, reprinted with permission.[128] Copyright 2014, OSA; b) PhC designs with maximized PBG. Reproduced with permission.[129] Copyright 2018, Wiley-VCH Verlag GmbH & Co. KGaA.

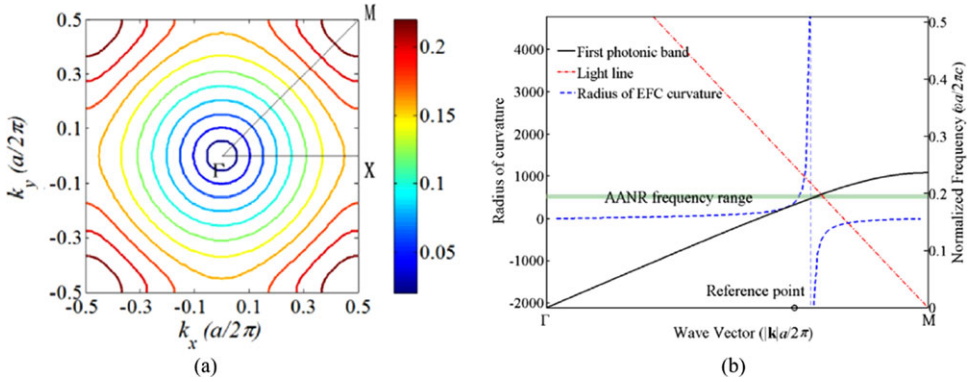

Figure 7. a) EFC of the first photonic band (unit of frequency is $2\pi c/a$). b) Upper and lower limit of the AANR frequency range and the reference point used in optimization (for interpretation of the references to color in this figure, the reader is referred to Meng et al.[130]). Reproduced with permission.[130] Copyright 2016, Elsevier.

suggested for the flat lens design that can achieve broadband sub-wavelength focal imaging as shown in Figure 8e,f.

2.2.3. Photonic Functional Structures and Devices

Photonic devices are traditionally designed by starting with an analytically designed structure and hand-tuning a few parameters.[132] By searching the full design space, topology optimization is able to produce photonic structures and devices with better performance and characteristics of interest than those of traditional ones. To date, a wide range of photonic devices have been designed by topology optimization, including slow light,[133] waveguides,[112,134,135] and filters.[136]

One challenge for the design of photonic devices is to ensure that the optimized irregular structures are still fabricable. Piggott et al.[137] introduced a general inverse design algorithm for nanophotonic devices that directly incorporates fabrication constraints. In their algorithm, an approximate minimum feature size was imposed by introducing additional curvature constraints on dielectric boundaries of the structure. Thereafter, by using a biasing technique in the optimization process, Su et al.[138] have designed and experimentally validated an optimized three-channel wavelength demultiplexer. **Figure 9** shows the simulated electromagnetic density at the operating wavelengths.

Liang and Johnson[139] presented a density-based topology optimization method to design finite-size photonic cavities with an enhanced Q/V ratio. In spite of the strongly enhanced

© 2019 WILEY-VCH Verlag GmbH & Co. KGaA, Weinheim

25130390, 2019, 7, Downloaded from https://onlinelibrary.wiley.com/doi/10.1002/adts.201900017 by The Librarian, Wiley Online Library on [03/06/2024]. See the Terms and Conditions (https://onlinelibrary.wiley.com/terms-and-conditions) on Wiley Online Library for rules of use; OA articles are governed by the applicable Creative Commons License

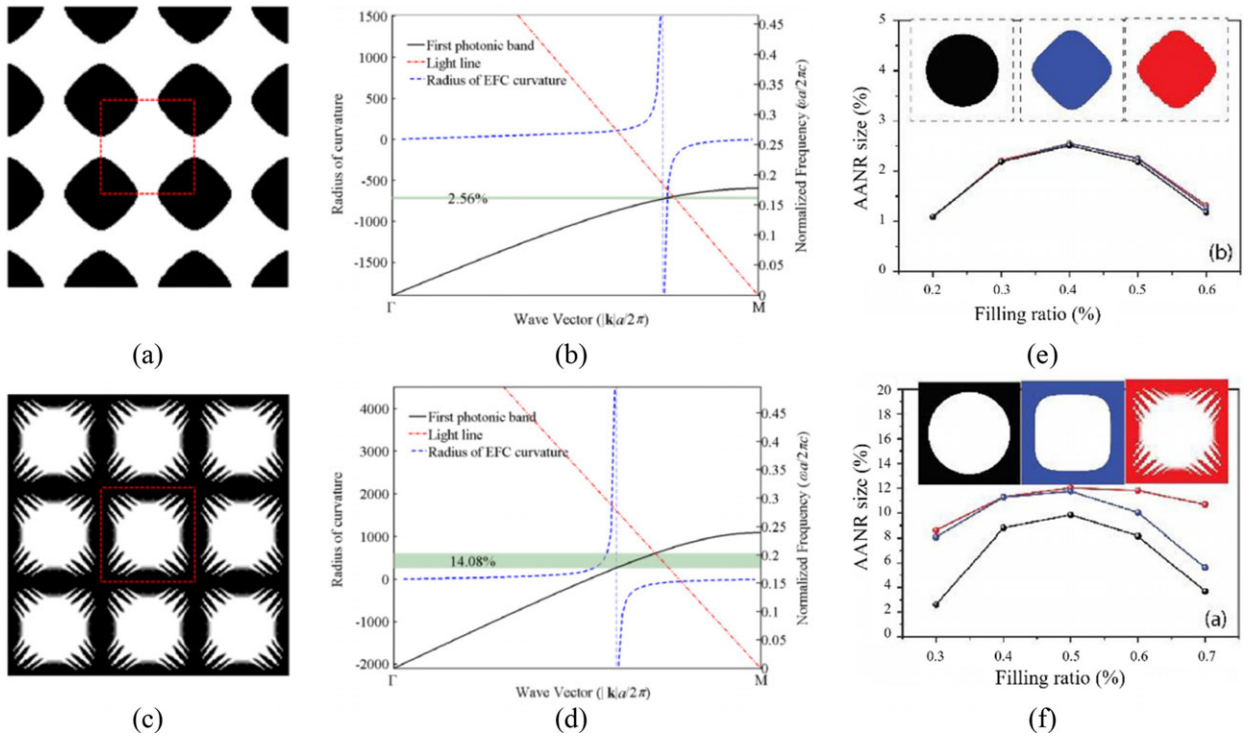

Figure 8. Optimized designs with 3 × 3 unit cells and band diagrams for a,b) TM mode and c,d) TE mode. The corresponding AANR frequency is indicated with the green area. e,f) AANR sizes versus filling ratios for the case of circle (black), supercircle (blue), and BESO optimization (red). The full width at half maximum of the focal spot of the flat lenses based on the "supercircle" unit cell for e) TM mode and f) TE mode. a–d) Reproduced with permission.[130] Copyright 2016, Elsevier. e,f) Reproduced with permission.[131] Copyright 2017, Elsevier.

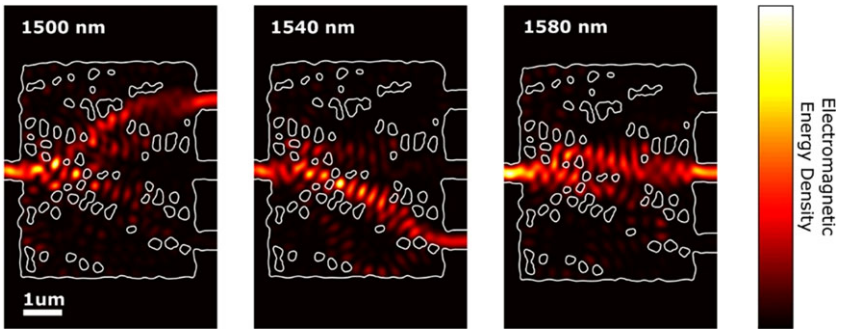

Figure 9. Three-channel wavelength demultiplexer. Simulated electromagnetic energy density in the device at the three operating wavelengths. Reproduced with permission.[138] Copyright 2018, American Chemical Society.

performance exhibited by their optimized photonic cavities, it is difficult to fabricate these structures due to the small holes or holes with irregular patterns and sharp features in the optimized structures. Recently, Wang et al.[140] implemented a density-based topology optimization method with manufacturing and length-scale control to design manufacturable 3D photonic membrane cavities. Based on the numerical results, the concept of an elliptic ring grating cavity was extracted by geometric fitting in their research. Dory et al.[141] reported the design of an efficient, scalable diamond photonic platform by using inverse design methods and quasi-isotropic etching techniques.[142] The quasi-isotropic etch enables the fabrication of various device geometries created by inverse design methods, which can have better performance than traditionally designed diamond photonics. This progress lays the foundation for scaling to larger quantum networks[143] with spins[144] embedded in quantum nodes. Callewaert et al.[145] utilized a computational inverse design method to design a stretchable meta-lens comprised of disconnected polymeric blocks with tunable focal distance. The meta-lens was made of seven blocks connected by two rubber bands, which acted like a stretchable platform. The device can be stretched along the Y direction by a factor up to s = 1.5. The stretching factor refers to the ratios between the total length after stretching and the designed length in Y dimension. Results of the inverse-designed device are shown in **Figure 10**, together with a Fresnel lens that has the same refractive index, matching size, focal distance, and operating wavelength. The focusing efficiency is defined as the ratio of the power that passes through

© 2019 WILEY-VCH Verlag GmbH & Co. KGaA, Weinheim

25130390, 2019, 7, Downloaded from https://onlinelibrary.wiley.com/doi/10.1002/adts.201900017 by The Librarian, Wiley Online Library on [03/06/2024]. See the Terms and Conditions (https://onlinelibrary.wiley.com/terms-and-conditions) on Wiley Online Library for rules of use; OA articles are governed by the applicable Creative Commons License

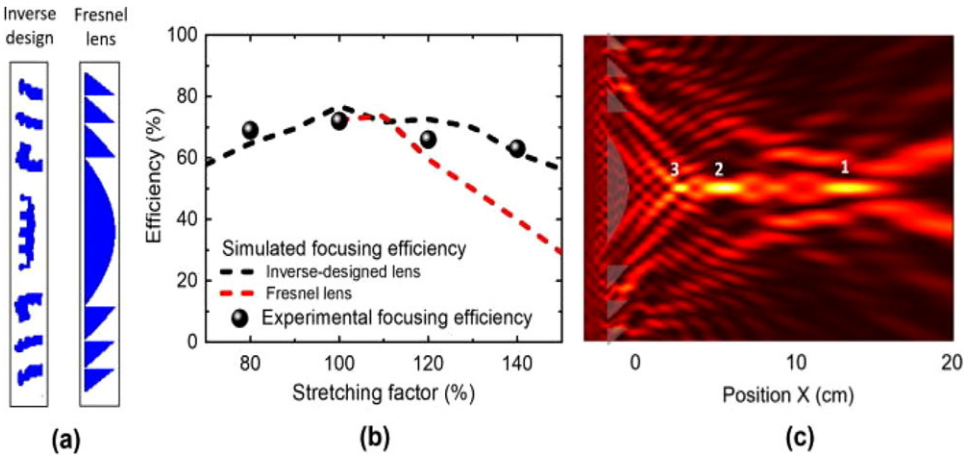

Figure 10. a) A Fresnel lens and the inverse-designed device. b) Experimental (spheres) and simulated (black dashed line) focusing efficiency of the inverse-designed device and the Fresnel lens (red dashed line) as a function of the stretching factor. c) Simulated optical power profile. Reproduced with permission.[145] Copyright 2018, American Institute of Physics.

an aperture in the focal plane with a size of the beam diameter over the total power going through the focal plane.

3. Phononic Crystals

PnCs can be constructed by two different types of materials, with relatively high contrast in their elastic properties, for example, mass density and Young's modulus. Recent research on PnCs tends to seek the optimized design with better performance (e.g., larger band gaps) for practical applications.

3.1. Properties and Applications of PnCs

Similar to the light manipulation in PtCs, PnCs can manipulate the propagation of elastic and/or acoustic waves. In some cases, the term of sonic crystals is adopted particularly referring to the control of acoustic waves. The propagation of acoustic/elastic waves within phononic band gaps will be prohibited. Sigalas et al.[146] noted that the existence of complete band gaps in PnCs is a result of the joint effect of the Bragg diffraction and the Mie scattering. Croënne et al.[147] investigated the generation of band gaps in PnCs and identified three different mechanisms, namely Bragg, hybridization, and weak elastic coupling effects. Among these mechanisms, Bragg interference is the most evident reason for phononic band gaps. Over the last two decades, PnCs have gained tremendous attention, and the analysis of PnCs has been developed extensively. The realization of a large band gap leads to a wide range of applications[148–160] in engineering and applied physics.

Inspired by the pioneering study on negative refraction of PtCs mentioned in Section 2.1, increasing efforts are devoted to investigating similar phenomena in PnCs and elastic/acoustic metamaterials, such as achieving negative refraction[161] and negative reflection[162] of acoustic waves. These theoretical and experimental explorations promote engineering devices with unconventional functions, such as focusing of sound waves[163] with high resolution. Analogous to the PtCs, there are also two different approaches to realize negative refraction in PnCs. One is exploiting the opposite direction of natural wave vector and energy flow at a high order band, typically at the second band, which has been extensively discussed in the literature.[164–166] This mechanism comes along with a backward-wave effect and the negative effective index, which is similar to the negative refraction by metamaterial. The other is to pursue negative refraction by intensive scattering of constituents, resulting in PnCs with positive effective properties that behave like normal right-handed materials. Such designs have advantages of single mode, high transmission, and possible AANR.[161]

3.2. Topology Optimization of PnCs

3.2.1. Phononic Band Gap Crystals

The application of phononic band gap crystals highly depends on the width of the band gap, and the key issue is therefore to engineer the phononic band gap as wide as possible. Sigmund and Jensen[167] first proposed a GTO method for systematically designing phononic band gap crystals. The goal of the optimization was to maximize the relative band gap size between two adjacent bands. The PnCs were composed of two material phases, and a linear interpolation was adopted to express the material properties. Topologies for both in-plane and out-of-plane waves could be obtained by using this method. It was found that the large contrast between the involved material phases was favored to yield large band gaps.

The optimization problem of PnCs designed by density-based approaches can be expressed similar to that of PtCs, where the propagation of elastic/acoustic waves is governed by Newton's second law rather than the Maxwell's equations for the propagation of electromagnetic waves in PtCs.

$$\rho\ddot{u} = \nabla(\lambda + 2\mu)(\nabla \cdot \mathbf{u}) - \nabla \times (\mu \nabla \times \mathbf{u}) \quad (4)$$

© 2019 WILEY-VCH Verlag GmbH & Co. KGaA, Weinheim

25130390, 2019, 7, Downloaded from https://onlinelibrary.wiley.com/doi/10.1002/adts.201900017 by The Librarian, Wiley Online Library on [03/06/2024]. See the Terms and Conditions (https://onlinelibrary.wiley.com/terms-and-conditions) on Wiley Online Library for rules of use; OA articles are governed by the applicable Creative Commons License

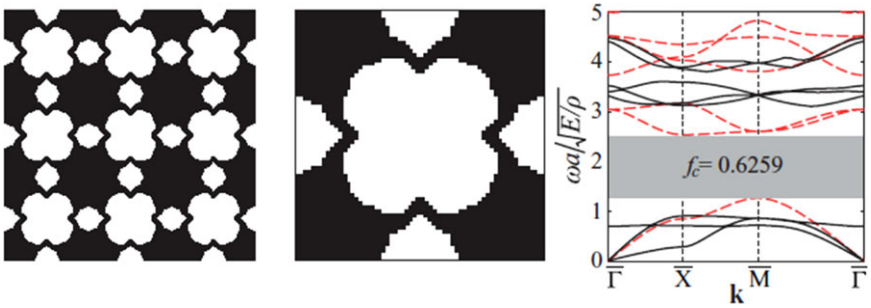

Figure 11. An optimized unit-cell design and band structure for combined out-of-plane and in-plane waves, lowest band gap. Reproduced with permission.[173] Copyright 2011, American Physical Society.

where λ and μ denote the Lame's coefficients, ρ is the material density, and $\mathbf{u}$ is the displacement vector. By applying the periodic boundary conditions and Bloch's theorem, the governing equation becomes an eigenvalue problem as follows:

$$\left(\mathbf{K}\left(\mathbf{k}\right)-\omega^{2}\left(\mathbf{k}\right)\mathbf{M}\right)\mathbf{u}\;=\;0 \tag{5}$$

where $\omega_j(\mathbf{k}_i)$ are the eigenvalues for the given wave vector $\mathbf{k}_i$, corresponding to the eigenvectors $\mathbf{u}_j(j\;=\;1,2,\ldots)$; matrix $\mathbf{K}$ and $\mathbf{M}$ are the global stiffness matrix and mass matrix. In topology optimization, Equation (5) is solved by finite element analysis.

To implement the GTO methods, the sensitivity analysis of eigenvalues can be calculated as

$$\frac{\partial\omega_j(\mathbf{k}_i)}{\partial x_e}=\mathbf{u}_j^{\mathrm{T}}\frac{\partial\left(\mathbf{K}-\omega_j^2\left(\mathbf{k}_i\right)\mathbf{M}\right)}{\partial x_e}\mathbf{u}_j \tag{6}$$

However, the sensitivity analysis becomes complicated when multiple eigenvalues occur. Take the case of a double eigenvalue with two corresponding eigenvectors (ω, $\mathbf{u}_1$, $\mathbf{u}_2$) as an example; the multiplicity of the eigenvalue implies that any linear combination of the eigenvectors $\mathbf{u}_1$and $\mathbf{u}_2$ (e.g., $c_1\mathbf{u}_1+c_2\mathbf{u}_2$) corresponding to ω will also satisfy the original eigenvalue problem. The sensitivities of double eigenvalues are eigenvalues of a 2D algebraic subeigenvalue problem.[168] Further investigation of the sensitivity of multiple eigenvalues is available in refs. [168–170].

The GTO method relies on the selected initial design with an existing band gap, of which the width is gradually enlarged by optimization. Conversely, the NGTO approach (e.g., GA) less depends on the initial guess but requires an extraordinary amount of computations for the evaluation of objective functions. The GA method has also been widely used to optimize phononic band gap structures. For instance, the GA method built on FEM was implemented to acquire the optimal design for acoustic waves propagating in both metal substrate (Ti/SiC) and porous media filled with fluid.[171] Hussein et al.[172] utilized the GA method to search the maximum gap widths of quadrate bi-material unit cells and also investigated the influence from the ratios of contrasting material properties. Their work was later extended to the study of PtCs and PnCs[91,173] with ultra-wide band gaps, respectively. Optimized topologies of the unit cell for in-plane waves, out-of-plane waves, and combined cases (see **Figure 11**) were presented, but only for the gaps at the first two bands. Hao-Wen et al.[174] utilized the fast non-dominated sorting-based genetic algorithm II (NSGA-II[175]) to perform the multi-objective optimization of 2D porous PnCs with simultaneously maximal band gap and minimal mass. To guarantee the self-support of cellular PnCs, an artificial geometrical constraint was adapted. Further, the multi-objective GA method was also used for the design of sonic wave attenuations.[176]

By using the modern BESO method starting from different initial designs, Li et al.[95] presented a series of optimized composite and cellular PnCs for propagation of in-plane (**Figure 12**), out-of-plane, and mixed waves, with gaps between adjacent bands, respectively. Meanwhile, Li et al.[177] conducted topology optimization by considering the maximization of band gap size and bulk/shear modules simultaneously. The static effective elasticity tensor of cellular PnCs was calculated by the homogenization method. The optimization problem was mathematically formulated with the objective to maximize the gap–midgap ratio and multiple constraints that included prescribed volume fraction and bulk/shear modulus. Thereafter, Zhang et al.[178] extended the method for the design of PnCs with sixfold symmetric hexagonal lattice. To address the fact that opening the band gap especially for in-plane waves due to the coupling of longitudinal and transverse waves is extremely difficult for topology optimization, Li et al.[179] proposed a simple way to create the gap between any two adjacent bands by employing different numbers of solid and hollow rods.

In addition to the complete band gap, the partial band gap of PnCs which can lead to the unidirectional transmission is also of practical value. Recently, Chen et al.[180] extended the BESO method to the design of PnCs for achieving unidirectional acoustic transmission (UAT). The PnCs will be placed at a bent rectangular tube with a bending angle equal to 45° (**Figure 13**a). To realize UAT, the incident waves from the right side should fall within the PBG of the PnCs, while those from the left side fall within the pass band. Hence, the optimization objective is to enlarge the minimum imaginary part of wave vectors along Γ-*X* (to create a phononic band gap) while keeping that along Γ-*M* less than the constraint value (to ensure an overlapped range of the PBG and the pass band). Novel designs of PnCs with such unique properties have been obtained, and numerical simulation results (Figure 13d,e) have been provided to prove their rectifying efficiency. He and Kang[181] studied the topology optimization of novel material microstructural configurations to achieve unidirectional elastic wave propagation by maximizing partial band gaps. In order to alleviate the issue of local optimum traps, they utilized the random morphology description functions to generate random initial designs for the optimization process.

© 2019 WILEY-VCH Verlag GmbH & Co. KGaA, Weinheim

25130390, 2019, 7, Downloaded from https://onlinelibrary.wiley.com/doi/10.1002/adts.201900017 by The Librarian, Wiley Online Library on [03/06/2024]. See the Terms and Conditions (https://onlinelibrary.wiley.com/terms-and-conditions) on Wiley Online Library for rules of use; OA articles are governed by the applicable Creative Commons License

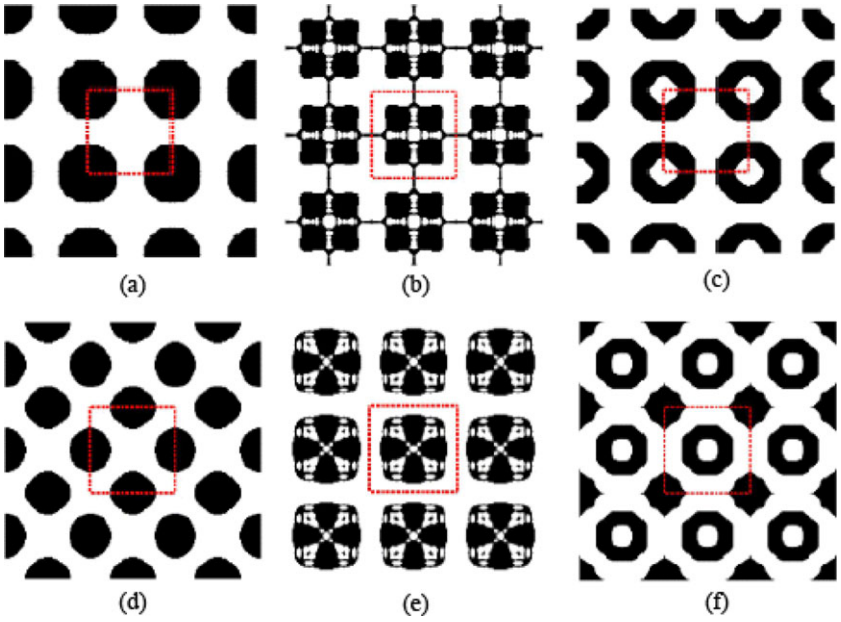

Figure 12. Optimized topologies for in-plane mode: a) the third band; b) the fourth band; c) the fifth band; d) the sixth band; e) the seventh band; f) the eighth band. Reproduced with permission.[95] Copyright 2016, Springer Nature.

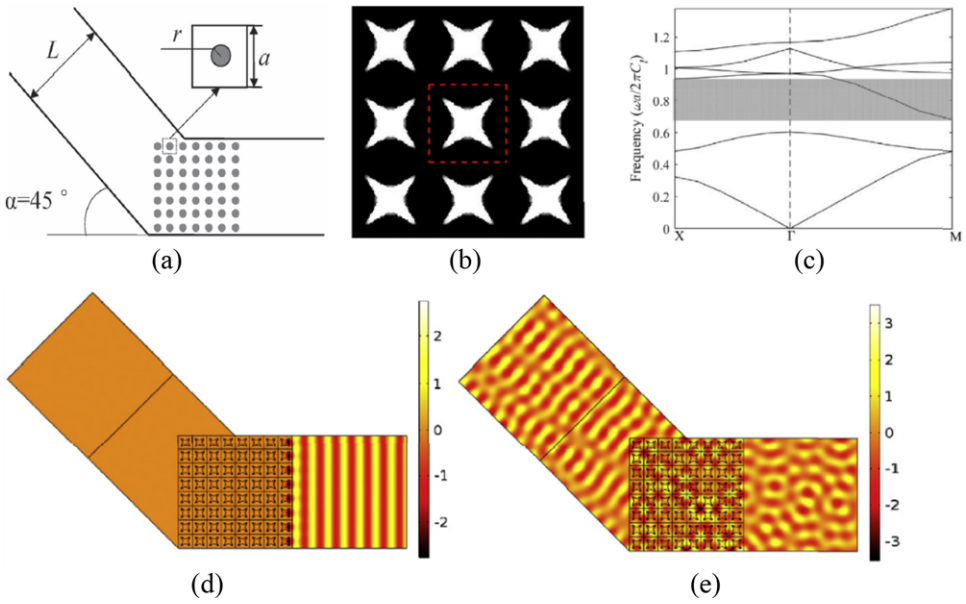

Figure 13. a) Schematic illustration of the 2D model of the UAT device. The device is assumed to be filled with air. The PnC consists of steel rods periodically arranged in the square lattice. b) An optimized topology (black, air; white, PVC) and c) its band diagram obtained under frequency $\Omega = 0.7$; the grey area represents the overlapped range of the PBG and the pass band. d) The corresponding pressure field for right and e) left incident waves. Reproduced with permission.[180] Copyright 2017, Elsevier.

Tremendous efforts have been devoted to the design of 2D phononic band gap crystals; however, topology optimization of 3D PnCs with omnidirectional band gaps, in which the elastic wave tensor equations must be retained, has rarely been investigated. Lu et al.[182] used a GTO method to optimize the symmetric structures of 3D PnCs consisting of tungsten–carbide and epoxy, with omnidirectional band gaps for the SC, BCC, and FCC lattices. In order to overcome the heavy burden of computation, the graphic processing unit (GPU) parallel computations were adopted in their work. Li et al.[183] developed a topology optimization algorithm to achieve the optimized band gap structures of 3D PnCs for elastic and acoustic waves, as shown in **Figure 14**.

Topology optimization methods have also been used for other properties in PnCs. For example, numerous studies have explored the properties of PnCs with linear elastic constituents, where the wave dissipation can be neglected. However, most

© 2019 WILEY-VCH Verlag GmbH & Co. KGaA, Weinheim

25130390, 2019, 7, Downloaded from https://onlinelibrary.wiley.com/doi/10.1002/adts.201900017 by The Librarian, Wiley Online Library on [03/06/2024]. See the Terms and Conditions (https://onlinelibrary.wiley.com/terms-and-conditions) on Wiley Online Library for rules of use; OA articles are governed by the applicable Creative Commons License

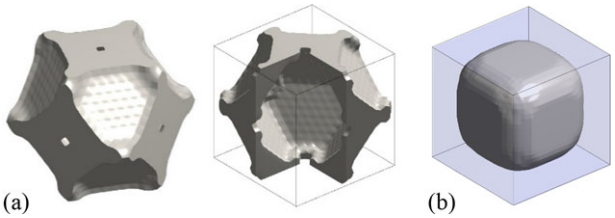

Figure 14. Optimized unit cell structures of PnCs for a) acoustic waves and b) elastic waves.

of the realistic materials such as rubber and epoxy, which are widely used as components of PnCs, exhibit viscoelastic behaviors. Since most realistic PnCs are dispersive and have losses, topology optimization of a PC should also consider its dispersive and dissipative effects. The effect of the viscoelasticity on wave dispersion has been studied in recent years.[184–186] Andreassen and Jensen[187] presented a GTO method to design periodic composites with dissipative materials for maximizing the loss/attenuation of propagating waves. A linear interpolation of the mass density and the real part of Young's modulus was adopted, while the quadratic interpolation was selected for the imaginary part. Chen et al.[188] investigated topology optimization of 2D viscoelastic PnCs for maximizing the minimum attenuation of waves propagating in all possible directions. Different from the traditional $\omega(\mathbf{k})$ approach, the $\mathbf{k}(\omega)$ approach[189] has been adopted. The optimization problem has been formulated to maximize the attenuation factor, which is characterized by the minimum of the imaginary part of wave vectors in all directions, subject to the bulk modulus and volume constraints. The resulting viscoelastic PCs have the maximum attenuation property of elastic waves at the specified frequencies, and meanwhile possess a prescribed stiffness.

In most research on topology optimization of PnCs, the design and analysis of PnCs are generally based on deterministic models. Nevertheless, the artificial PnCs have an uncertain spatial variation of material properties resulting from manufacturing processes, which has an impact on their band gap properties. Besides, the geometrical uncertainties arising from manufacturing errors and imperfections will also affect the real performance of PnCs. To address the problem of geometrical uncertainties, a level set–based robust shape and topology optimization framework was proposed by Zhang and Kang[190] Considering random-field material properties, Zhang et al.[191] developed a robust topology optimization method to design the microstructures of PnCs. The random material Young's modulus fields were discretized into several uncorrelated uncertain variables by using the expansion optimal linear estimation method. In their recent research,[192] a phase-field based robust topology optimization method has been proposed for PnC design considering uncertain diffuse regions between material phases. Xie et al. have also investigated the topology optimization of PnCs with uncertainties.[193,194] A sparse point sampling–based Chebyshev polynomial expansion (SPSCPE) method was proposed, in which the interval model was introduced to handle the unknown-but-bounded parameters.

Similarly, few works have been done for AANR of acoustic waves by optimized PnCs. In order to obtain the maximum operation frequency of AANR, Li et al.[195] introduced a topology optimization algorithm based on the BESO method for constructing a 2D solid/air PnC displaying AANR phenomenon. Their optimization results indicate that the modification of the geometry can effectively bring about a wide AANR frequency range even at a filling fraction as low as 20% (see **Figure 15**a). The optimized unit cells are shown in Figure 15b, and the dependence of the refracted angle and the incident angle at different frequencies is presented in Figure 15c. The wide frequency range of AANR and subwavelength focusing effect makes the proposed PnC a desirable candidate for the design of acoustic super lens.

3.2.2. Functional PnC Devices

Topology optimization approaches have also been used to create functional structures and devices with desired performance. Similar to the traditional structural design, a finite design domain with specified boundary conditions and external wave loading is considered.

Halkjær et al.[196] used the topology optimization method to design a single-material Mindlin plate with maximized band gap size for bending waves. Instead of the SIMP scheme, an explicit mesh-independent penalization scheme[197] was adopted as an extra constraint in their research. The optimized structures tended to be degenerated with disconnected beams and masses

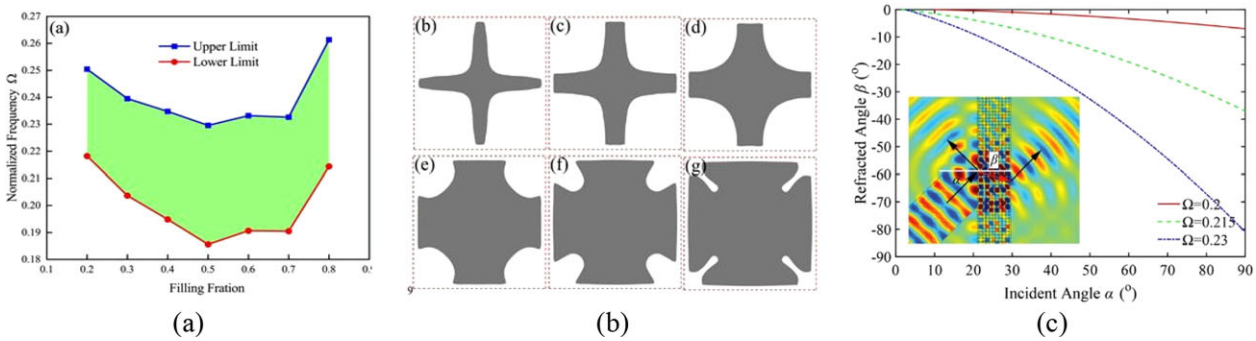

Figure 15. a) Optimized upper and lower limits of AANR frequency range as a function of filling fraction. b) Optimized unit cells with filling fraction of 20%, 30%, 40%, 60%, 70%, and 80%, respectively. c) The refracted angle as a function of incident angle at different normalized frequencies. Reproduced with permission.[195] Copyright 2017, Nature Research.

© 2019 WILEY-VCH Verlag GmbH & Co. KGaA, Weinheim

25130390, 2019, 7, Downloaded from https://onlinelibrary.wiley.com/doi/10.1002/adts.201900017 by The Librarian, Wiley Online Library on [03/06/2024]. See the Terms and Conditions (https://onlinelibrary.wiley.com/terms-and-conditions) on Wiley Online Library for rules of use; OA articles are governed by the applicable Creative Commons License

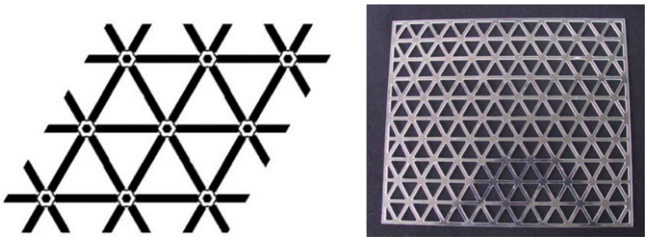

Figure 16. The fabricated periodic plate (right) made of polycarbonate consisting of 10 × 10 base cells (left). Reproduced with permission.[196] Copyright 2006, Springer Nature.

while maximizing the relative band gap size. In order to improve the practicality of optimized structures, the objective function was modified as the absolute gap size multiplying the square of the mean gap frequency. To further experimentally investigate the dynamic properties, a finite plate as shown in **Figure 16** was fabricated based on the design of the unit cell. The experimental data showed good agreement with the theoretical results. Such a periodic structure can be useful in practical situations where the minimization of the vibrations transferred to the surroundings is required.

Taking the stiffness of porous PnC plates into account, Hedayatrasa et al.[198] utilized the multiple objective GA method NSGA-II to optimize thin and thick porous PnC plates with maximal relative band gap size of flexural-guided wave modes. In order to maximize the effective in-plane stiffness, the minimization of the strain energy compliance of the unit cell was defined as the second objective function. In their subsequent work,[199] an improved and more efficient topology optimization algorithm was presented. A subset of promising compliant and stiff topologies were fabricated and their band gap stiffness efficiencies were validated experimentally.

With the development in nano- and micro-manufacturing processes, the design of surface wave devices has attracted much attention in recent years. Rupp et al.[200] proposed a topology optimization approach to design the surface wave devices, especially filters and waveguides composed of phononic materials. They employed the linearized elasticity equations to construct the objective function for minimizing displacements in certain regions of the design domain. Nonreflecting boundary conditions, that is, viscous damping and perfectly matching layers, were imposed wherever the semi-infinite computational domain was cut. The optimization problems were solved by using the method of moving asymptotes[201] and the commercial large-scale sequential quadratic programming method implementation SNOPT. Three phononic devices (a 3D Bragg grating, a 2D patterned thin film surface wave filter, and a 3D surface waveguide) consisting of silicon and aluminium were obtained and validated by simulations in their research. Thereafter, Rupp et al.[202] investigated the wave propagation phenomena in a polarization-patterned piezoelectric plate that was uniformly covered by electrodes. Four switchable applications (i.e., a filter, a waveguide, an energy harvester, and a wave actuator) could be actively switched off/on by either connecting or disconnecting the electrodes. The piezoelectric polarization patterns in this phononic device were determined by topology optimization rather than intuitive design.

4. Metamaterials

Recent developments in the synthesis and novel fabrication technique have enabled the construction of composite materials that mimic known material responses or that have new realizable response functions, which do not occur or not be readily available in nature.[203] In this section, electromagnetic and acoustic/elastic MMs acting as wave-propagating mediums with exceptional properties will be introduced.

4.1. Electromagnetic Metamaterials

4.1.1. Properties and Applications of EM Metamaterials

An electromagnetic metamaterial can be designed by embedding various inclusions in some matrix material with a spatial periodic distribution, and its lattice constant is much smaller than the wavelength of the incident wave. In the composite medium, electromagnetic waves interact with the inclusions, which in turn affects the macroscopic properties such as the effective permittivity ε and permeability μ of this medium. If a material had negative values for both the electric and magnetic response functions (i.e., $\varepsilon < 0$, $\mu < 0$) at certain frequencies, then its index of refraction would be negative too. This concept has gained considerable attention in the last two decades.[13,16,75,203–206] In order to depict this concept mathematically, Ziolkowski and Heyman[207] investigated the propagation of electromagnetic waves in the double negative (DNG) medium by using both analytical and numerical techniques. The choice of the square root that produced a negative refractive index and positive wave impedance was highlighted in their research.

Both the isotropic and anisotropic MMs can give rise to these special properties. There is a class of EM metamaterial with extreme anisotropy, namely hyperbolic metamaterials. They can display hyperbolic dispersion, in which one of the principal components of their permittivity or permeability tensors has the opposite sign to the other two principal components.[208]

On the other hand, PtCs introduced in Section 2 can also exhibit extraordinary electromagnetic responses without resonator elements that are typical to MMs.[209] For example, two cases of PtCs behaving as metamaterials are reviewed by Foteinopoulou.[210] In the sense of possessing effective photonic properties, however, PtCs do not necessarily act as metamaterials. The problem is how to distinguish PtCs and dielectric MMs when their parameters (e.g., permittivity and lattice constant) vary continuously. Rybin et al.[211] theoretically and experimentally investigated the transition from PtCs to dielectric metamaterials. The concept of a phase diagram based on the physics of Mie and Bragg resonances was proposed in their study. Their results indicated that a periodic photonic structure transferred into a metamaterial when the Mie gap unfolded below the lowest Bragg band gap where the homogenization approach could be justified and the effective permeability became negative.

The materials contributing to an individual cell of EM metamaterials do not exhibit those negative properties, but the overall structure of such periodic arrays can be considered as an effectively homogeneous EM material that exhibits effective negative properties. Analogous to electromagnetic properties

© 2019 WILEY-VCH Verlag GmbH & Co. KGaA, Weinheim

25130390, 2019, 7, Downloaded from https://onlinelibrary.wiley.com/doi/10.1002/adts.201900017 by The Librarian, Wiley Online Library on [03/06/2024]. See the Terms and Conditions (https://onlinelibrary.wiley.com/terms-and-conditions) on Wiley Online Library for rules of use; OA articles are governed by the applicable Creative Commons License

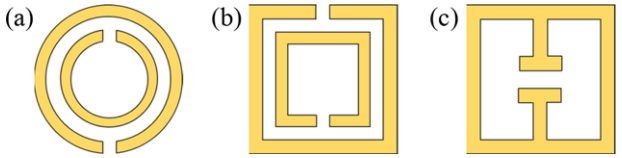

Figure 17. a) Circular structure SRR; b) squared structure SRR; c) ELC resonator.

exhibited by a solid metal in the near ultraviolet (UV), Pendry et al.[212] proposed a metallic microstructure consisting of thin and infinitely long metal wires, which had a negative permittivity below plasma frequency. Another microstructure, the split-ring resonator (SRR) (**Figure 17**a,b) in which an incident light field induced a circulating and oscillating electric current that generated a magnetic dipole moment normal to the ring, was also proposed by Pendry et al.[15] and a wide range of permeability was achieved. The periodic arrangement of the resonators leads to strong magnetic coupling of the units and an effective permeability μ_{eff} which can be approximated by the expression

$$\mu_{\text{eff}}\ (\omega) = \mu'\ (\omega) + i\mu''(\omega) \tag{7}$$

where μ_{eff} is a complex function of the frequency of incident radiation, with real part μ' and imaginary part μ''.

Schurig et al.[213] investigated the fundamental issues in the application of effective negative index (NI) media based on the SRR and wire media. They introduced an electric-inductive-capacitive (ELC) resonator (Figure 17c) which was suitable for implementing media with desired positive or negative permittivity in 1D, 2D, and 3D. Later, various types of resonators were suggested for building EM metamaterials such as thin metallic wires,[214] electric ring resonator,[215] Swiss rolls,[216] fishnet structures,[217,218] and other periodic structures composed of high-permittivity dielectric elements[219,220] which could deliver an effective magnetic response.

On the basis of unique properties, for example, the anomalous refraction, super lensing, the change of the light polarization state, the ability to slow down light,[221] remarkable development has been achieved in the application of electromagnetic MMs in every technologically relevant spectral range from radio to the near optical. A variety of EM devices made of metamaterials have been presented, including subwavelength optical waveguides,[222] superlens,[75,223,224] absorbers,[225–229] and cloaks.[230–238]

4.1.2. Topology Optimization of EM Metamaterials

Most metamaterials with negative permeability are realized based on variations of the SRR arrangement after the publication of Pendry et al.[15] In order to explore alternative designs of microstructures beyond the classical SRR-inspired layouts, Diaz and Sigmund[239] proposed a topology optimization method for the design of negative permeability metamaterials, using a SIMP-like model and the *S*-parameter retrieval method[240] to compute the effective property. The imaginary part of the effective permeability was chosen as the objective function to be minimized at a given frequency in the optimization problem. As shown in **Figure 18**a, the unit cell is a parallelepiped with a centrally located inclusion. Several designs for metallic structures attached to dielectric substrates with negative permeability were provided to prove the sufficiency of this approach (see Figure 18b,c). Their topology optimization method was also demonstrated as a systematic design method for metamaterial design.[241]

For the topological design of MMs, a negative effective property, permeability/permittivity or density/stiffness, is the result of a resonance phenomenon. To illustrate the simple model of electromagnetic metamaterials in Equation (7), when a resonance ω_0 occurs at a frequency near the target frequency Ω^0, there will be a region of negative μ' at Ω^0.[239] To obtain metamaterials with negative permeability, one would seek designs that have a resonance

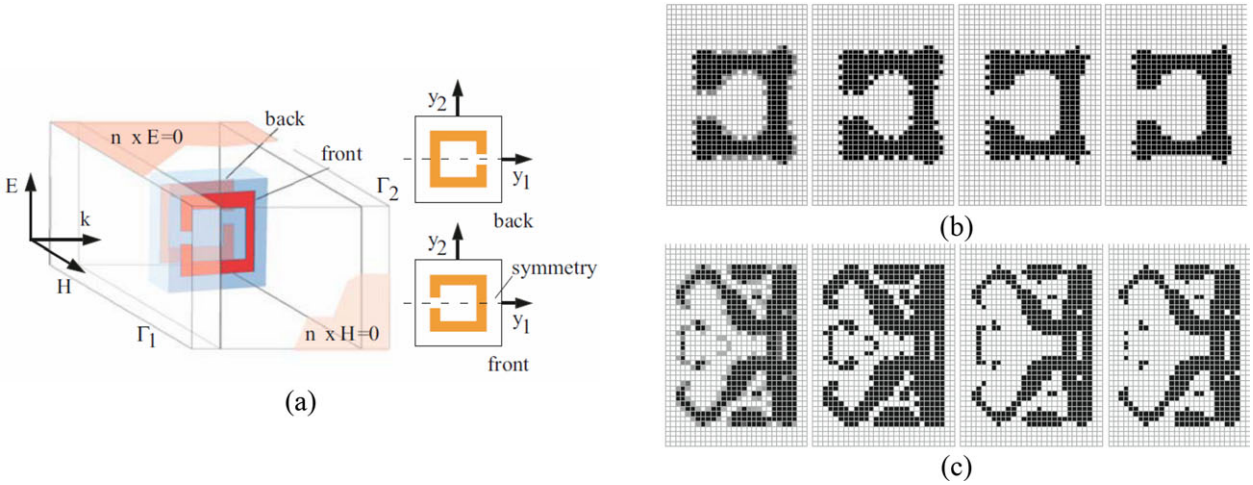

Figure 18. a) A representative cell. A thin layer of copper is printed on one face of the inclusion plate, and another layout rotated 180° about the vertical axis is printed on the opposite face. b) From left to right, a possible solution at the target frequency of 2.2 GHz and post-processing with various thresholds 0.3, 0.5, 0.7. c) From left to right, a possible solution at the target frequency of 3.0 GHz and post-processing with various thresholds 0.3, 0.5, 0.7. Reproduced with permission.[239] Copyright 2009, Springer Nature.

© 2019 WILEY-VCH Verlag GmbH & Co. KGaA, Weinheim

25130390, 2019, 7, Downloaded from https://onlinelibrary.wiley.com/doi/10.1002/adts.201900017 by The Librarian, Wiley Online Library on [03/06/2024]. See the Terms and Conditions (https://onlinelibrary.wiley.com/terms-and-conditions) on Wiley Online Library for rules of use; OA articles are governed by the applicable Creative Commons License

frequency in this neighborhood. $\mu'(\Omega^0)$ or $\mu''(\Omega^0)$ are then used directly as the objective function

$$\min : f(x_e) = \mu'(\Omega^0) \text{ or } \mu''(\Omega^0) \tag{8}$$

To characterize the effective properties of electromagnetic MMs, such as effective permeability and effective permittivity, three types of approaches can be implemented:[242] homogenization methods, field averaging approach,[243] and the S-parameter retrieval method.[244] The homogenization method (e.g., the energy-based method[245]) can be used only when the periodic unit cell can be regarded as infinitely small compared to the wavelength. The field averaging approach derives the effective medium properties based on the relation of electric field **E** and electric flux density **D**, as well as the magnetic field **H** and magnetic field density **B**, which can be obtained from integral form of Maxwell's equations. The S-parameter-based approach was originally proposed by Smith et al.[244] and further improved in the references.[240,246] The effective properties computed by this approach, namely the complex transmission and reflection coefficients, were widely adopted in the topology optimization of MMs.[239,242,247]

Zhou et al.[248] introduced a level set–based topology optimization method to the design of EM metamaterials, in which the interface between the vacuum and metal phase was expressed by the zero-level contour of a scalar level set function. To simplify the optimization, the electric field integral equation rather than the typical Maxwell's equations was adopted as governing equation, and it was solved by the method of moment[249] in an adaptive triangular mesh. The objective function was defined in terms of the current norm and the norm direction of the level set function. However, this objective function was not explicitly related to the effective electromagnetic properties. In their subsequent work,[247] the effective permeability computed by the *S* parameters[250] was directly used in objective functions. The FDTD method was also applied to solve the vector wave equation (one type of the Maxwell's equation) and its adjoint system. Novel structures were obtained with negative permittivity and permeability in specific frequency ranges by using this improved method.

Otomori et al.[242] presented a topology optimization method for the design of negative permeability dielectric metamaterial using the level set method and FEM. The effective properties were computed based on the *S*-parameter approach. Two optimization problems were considered in their research, one of which was to find a distribution of dielectric material within the fixed domain that minimized the effective permeability, and it could be formulated as a problem to minimize the effective permeability at a prescribed frequency. The other one was to find a distribution of dielectric material that had an expected value of effective permeability, which was formulated to minimize the square of the difference between the effective permeability and a prescribed value at a prescribed frequency. Numerical examples for both 2D and 3D cases were provided to prove the validity of their method. Later, the same research group (Otomori et al.) used the level set–based topology optimization method to successfully design an electromagnetic cloak,[251] as well as an optical hyperlens[252] made of hyperbolic metamaterials, in which the energy-based homogenization method[253,254] was applied for the computation of the effective permittivity.

In recent years, the availability of nanometer-scale fabrication techniques has motivated scientists to explore subwavelength-structured metamaterials with designed optical properties at much shorter wavelengths, for example, in the infrared and visible regions of the spectrum.[255] An ultra-compact wideband on-chip polarization rotator with a low conversion loss of 2 dB and high extinction ratio of 10 dB has been designed and experimentally realized by Yu et al.,[256] using a genetic algorithm. Based on the optimized results, the device fabrication involved only a single step of electron-beam lithography with subsequent dry etching on the silicon-on-insulator (SOI) wafer. Shen et al.[257] demonstrated an integrated-nanophotonics polarization beamsplitter through a nonlinear optimization algorithm based on direct-binary search (DBS). Starting from a randomly chosen pixel distribution, the geometry of the metamaterials was allowed to be freely optimized according to the figure-of-merit, which was defined as the average transmission efficiency for TE and TM polarization states. The high computational cost can be resolved by a variety of approaches to parallelize and increase the efficiency. The device was patterned in the top silicon layer of an SOI substrate (**Figure 19**a). TM and TE components of the input light are coupled into the top and bottom output waveguides (Figure 19b,c). Besides, Menon et al. applied this DBS-based optimization method to design many other devices, such as metamaterial couplers for waveguides,[258] free-space metamaterial polarizers,[259] and light-trapping nanostructures.[260] Lu et al.[261] utilized an asymmetrical DBS algorithm to successfully design a colorless 3 dB coupler.

Dirac cones in PtCs have attracted considerable attention due to their connections to novel optical properties, such as *Zitterbewegung* of photons,[262] effective zero-index behavior,[263–265] topologically protected states,[266] and exceptional points.[267] The Dirac cones in PtCs can be classified as deterministic Dirac cones and accidental Dirac cones.[268] The deterministic Dirac cones are formed at the boundary of Brillouin zone, while accidental Dirac cones are degenerated at the center of Brillouin zone and can be further classified as second-order Dirac-like cone (single-polarization and dual-polarization), third-order Dirac-like cone, and double Dirac cone. PtCs with second-order Dirac-like cones can be regarded as double zero index MMs. Lin et al.[269] extended the optimization formulation for a single resonant mode to a multi-mode degeneracy. By maximizing the minimum of a collection of the local density of states corresponding to different sources at the given frequency, the MMs with third-order Dirac-like cones[270] and dual-polarization Dirac-like cones[269] were successfully obtained. Chen et al.[271] investigated the design of MMs with Dirac-like cones using a two-stage topology optimization approach. Dirac-like cones formed by the degeneracy of doubly degenerate modes (dipolar modes) and a single mode (monopolar or quadrupolar mode) at different desired frequencies were successfully obtained for both TM mode and TE mode. Based on the optimized structures, exotic wave manipulation properties associated with Dirac-like cones, such as cloaking, wavefront shaping, and tunneling through bent channels, were exhibited through full wave simulation.

© 2019 WILEY-VCH Verlag GmbH & Co. KGaA, Weinheim

25130390, 2019, 7, Downloaded from https://onlinelibrary.wiley.com/doi/10.1002/adts.201900017 by The Librarian, Wiley Online Library on [03/06/2024]. See the Terms and Conditions (https://onlinelibrary.wiley.com/terms-and-conditions) on Wiley Online Library for rules of use; OA articles are governed by the applicable Creative Commons License

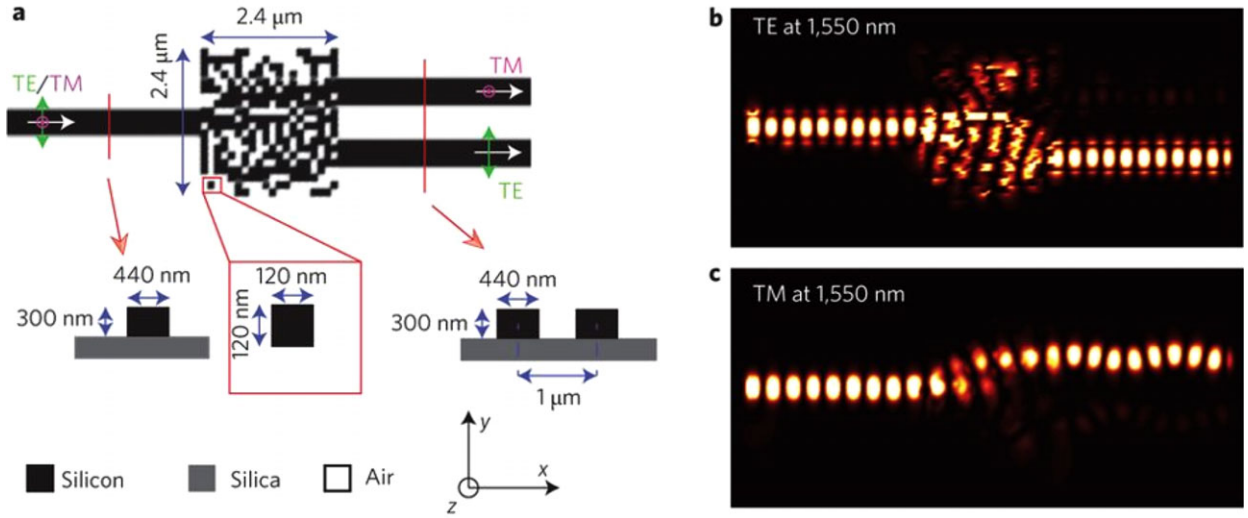

Figure 19. The polarization beamsplitter. a) Geometry of the device. b) Simulated steady-state intensity distributions for TE and c) TM polarized light at the design wavelength of 1550 nm. Reproduced with permission.[257] Copyright 2015, Nature Research.

4.2. Elastic/Acoustic Metamaterials

As the counterpart of electromagnetic metamaterials, E/A metamaterials offer the possibility to manipulate the propagation of elastic/acoustic wave in the subwavelength scale through different mechanisms. The semantic frontier between PtCs/PnCs and metamaterials is illustrated by Craster and Guenneau[272] as "low-frequency high-contrast and high-frequency homogenization models for periodic structures, the former being well suited for metamaterials, while the latter discloses the band structure and associated anomalous dispersion of PCs."

4.2.1. Properties and Application of E/A Metamaterials

Inspired by the realization of the effective negative index medium for EM waves, a "double-negative" material is possible for elastic/acoustic waves. The refractive index n for elastic materials can be given by

$$n = -\sqrt{\frac{\rho}{X}} \tag{9}$$

where ρ is the mass density, $X = G$ for the transverse wave or $X = E \equiv K + 4G/3$ for the longitudinal wave, with G and K being shear modulus and bulk modulus, respectively.[17] The velocity of the longitudinal waves is governed by $v_l = \sqrt{E/\rho}$. Negative refraction can be realized if both the mass density and the elastic constants become negative in the same frequency range. However, no natural materials are found to have a negative mass density or a negative elastic constant. Therefore E/A metamaterials are created artificially by assembling periodic microstructures consisting of conventional materials, such as metals or plastics. The extraordinary properties of metamaterials come from their microstructures rather than the material composition.

In the context of E/A metamaterials, negative mass density means the spatially averaged force is opposite to the acceleration in phase at given frequencies, and materials constructed by such microstructures can exhibit macroscopic dynamics that deviates from Newton's second law.[273] In acoustics, the first metamaterial was fabricated with rubber-coated spheres to create locally resonant and subwavelength structures, behaving as a material with effective negative elastic constants.[274] Summarized by Lai et al.[21] and Wu et al.,[18] negative mass density can result from dipolar resonances, while certain elastic moduli are related to monopolar and quadrupolar resonances. There are several designs for metamaterial unit cells[19,275,276] proposed to display different monopolar, dipolar, quadrupolar, and rotational responses. It is possible to achieve DNG effective properties by combining two structures supporting different resonances, or by constructing a structure that simultaneously displays overlapping responses. Currently, much effort has been devoted to the interesting wave phenomena in elastic/acoustic metamaterials, for example, negative mass density and/or stiffness.[277–282] Similar to the hyperbolic EM metamaterials described in Section 4.1.1, anisotropic metamaterials for elastic/acoustic wave control[283–285] have also been investigated. Due to the exotic properties, E/A metamaterials have been developed for diverse applications in science and engineering, for example, the amplification,[22] blast-wave impact mitigation,[286] subwavelength focusing, and[287] cloaks.[288–290] More examples on this topic can be found in refs. [291,292].

4.2.2. Topology Optimization of E/A Metamaterials

Many intriguing and effective metamaterial structures have been suggested by physicists and engineers, based on their intuition and experience. Nevertheless, the topology optimization method, as a systematic design method introduced in previous sections, is required when it comes to taking full advantage of the possibilities of MMs.

Li et al.[293] demonstrated a GA approach for optimizing the effective material parameters of an acoustic metamaterial. The

© 2019 WILEY-VCH Verlag GmbH & Co. KGaA, Weinheim

25130390, 2019, 7, Downloaded from https://onlinelibrary.wiley.com/doi/10.1002/adts.201900017 by The Librarian, Wiley Online Library on [03/06/2024]. See the Terms and Conditions (https://onlinelibrary.wiley.com/terms-and-conditions) on Wiley Online Library for rules of use; OA articles are governed by the applicable Creative Commons License

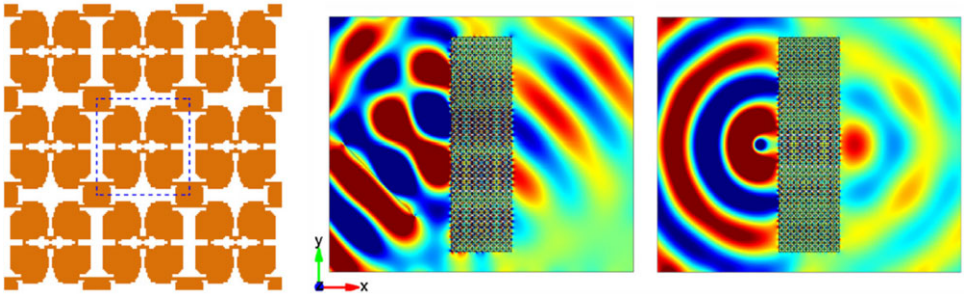

Figure 20. a) An optimized elastic metamaterial with the unit cell marked by the dashed line. b) The displacement field of the L-wave (at 18 kHz) component generated by an incident Gaussian beam (45°). c) The imaging field pattern with the source located from the left side of the slab. Reproduced with permission.[299] Copyright 2017, Elsevier.

fitness function for evaluation of the unit cell's performance was formulated based on three objectives: maximization of the refractive index, minimization of the unit cell's impedance, and minimization of the frequency dependence. Lu et al.[294] conducted a level set–based topology optimization for the design of acoustic metamaterials with negative bulk modulus. The optimization problem was formulated to find a material distribution that minimized the real part of the effective bulk modulus computed by the S-parameter-based approach at a given frequency. Christiansen and Sigmund[295] presented a topology optimization–based approach for designing acoustic metamaterial slabs that exhibit a prescribed negative refraction at a desired angle of incidence and target frequency. The refractive index derived from Snell's law may not be consistent with the definition given as $n = c/c_p$, where c is the wave speed in vacuum and c_p is the velocity of the wave propagating through the medium. Thus, it is possible for the negative refractive waves to be achieved without the resulting field having a negative phase velocity inside the slab. The corresponding experimental validation was reported.[296] Furthermore, by adjusting the relevant material parameters, this approach is also applicable to electromagnetic and elastic wave problems modeled by the Helmholtz equation.

Inspired by the previous studies on acoustic MMs, Dong et al.[297] has developed a unified topology optimization framework to systematically design and realize DNG acoustic metamaterials, with consideration of several structural and physical characteristics, such as type of the unit cell's symmetry (i.e., square, chiral, and orthogonal symmetries), minimal geometrical size, and dispersion extents of effective parameters. Due to the high contrast in the constituent materials (solid/air), the solid can be taken as a fluid with very high stiffness and specific mass while formulating the wave equations. The commonly accepted approach of extracting the acoustic effective properties from reflection and transmission[298] has been adopted to characterize the MMs. Based on the topology optimization results, they have investigated two categories of microstructures with broadband DNG properties, namely the resonance cavity–based and space-coiling. A feasible design principle for resonance cavity–based structures suggested by them is to properly assemble the multiple air resonant cavities, several solid blocks, and air channels. Expected negative refraction and subwavelength imaging of the space-coiling designs have been numerically and experimentally validated.

The genetic algorithm (GA) has also been adopted by Dong et al.[299] to construct the anisotropic elastic MMs with broadband DNG effective material properties for longitudinal waves in a prescribed frequency range. The optimization objective function was formulated for maximizing the difference between the minimal and the maximal positive effective parameters at sampling frequencies to design the orthotropic microstructure. Their optimized anisotropic MMs are comprised of elastic solid block and narrow connections (**Figure 20**a) with typical local resonance characteristics.[174] The negative wave refraction and imaging of longitudinal waves have been achieved by the optimized results (Figure 20b,c). According to their analysis, the DNG effective material properties are induced by the quadrupolar or multipolar resonances. Afterwards, Dong et al.[300] implemented the GA-based method and the effective medium theory to design the single-phase hyperbolic MMs for super-resolution imaging. From their results, the strongly anisotropic effective mass density with negative values along one direction in the deep subwavelength frequency range can be guaranteed by the special multipolar resonances. The presented hyperbolic MMs exhibit several novel undiscovered structural topologies and are proved to support the subwavelength imaging.

However, metamaterials with local resonant structures usually have high damping loss, which is unexpected in some applications. Recently, Rong and Ye[301] presented a two-step density-based topology optimization design scheme for non-resonant hyperbolic elastic metamaterials. The first is to obtain the desired wave mode by maximizing a directional band gap where waves are permitted to propagate in only one direction. The frequency band is then fixed. In the second step, the curvature of the equal-frequency contour is optimized to achieve the convex shape that is responsible for producing negative refraction. The MMs optimized by this scheme exhibit highly anisotropic and polarization-dependent transmission properties.

Although a lot of progress has been made in this field, the topology optimization of metamaterials is still in its infancy, and substantial work is required to make it more versatile and effective in accommodating various specific design issues.

© 2019 WILEY-VCH Verlag GmbH & Co. KGaA, Weinheim

25130390, 2019, 7, Downloaded from https://onlinelibrary.wiley.com/doi/10.1002/adts.201900017 by The Librarian, Wiley Online Library on [03/06/2024]. See the Terms and Conditions (https://onlinelibrary.wiley.com/terms-and-conditions) on Wiley Online Library for rules of use; OA articles are governed by the applicable Creative Commons License

5. Conclusions

Massive attention has been drawn to the study of wave propagation in periodic medium since pioneer works about electronic wave functions and quantum mechanics more than a century ago. With the emergence of artificial periodic materials and the development of numerical methods, the past decades have witnessed a renewed interest in this thrilling subject. In this paper, we have introduced various properties of PtCs/PnCs and metamaterials, which mainly come from their microstructures rather than the material composition. Based on those required properties, the design of such structural materials can be converted to a typical topology optimization problem by searching the optimal distribution of constituent materials within a given domain. This paper has reviewed the recent development of topology optimization on designing PtCs, PnCs, and MMs with desired properties and functionalities.

In spite of the wide application of topology optimization methods for designing PtCs, PnCs, and MMs, the fabrication technologies employed for these designs are still in a preliminary stage. Some of the optimized structures are difficult or even impossible to manufacture. For the density-based topology optimization algorithms, the final design may contain many intermediate elements which causes the difficulty of accurately determining structural boundary. On the other hand, even for a clear 0/1 design, the post-processing is still necessary when there are zig-zag boundaries. In this aspect, the optimized design from the LS method potentially provides a smooth and crisp boundary description. On the other hand, the investigation on the experiments of optimized designs is relatively rare. To exploit the full potential of topology optimization technique in designing PtCs, PnCs, and MMs, further research and cross-discipline cooperation should be devoted to this field.

Both GTO and NGTO methods are widely used in the design of structural materials. NGTO does not need to conduct sensitivity analysis and can be easily applied for any new problems. Compared with GTO approaches, the computational efficiency of NGTO should be further improved for topology optimization. Since topology optimization problems are highly nonlinear and non-convex, both GTO and NGTO cannot guarantee a global optimum as demonstrated by Sigmund.[302] The theoretical limits of physical properties, for example, the Hashin–Shtrikman bounds[303] of effective permittivity and permeability, physical bounds on optical response in absorptive structures[304,305] provide valuable guides for verifying the optimized solutions resulting from topology optimization. However, physical properties under dynamic condition may exceed those theoretical bounds, for example, the effective permittivity of electromagnetic metamaterials may attain a negative value. From the perspective of practical application, the significance of topology optimization lies in creating a structure of PtCs, PnCs, and MMs with desired properties. The methodology of material design via topology optimization reviewed in this paper will be of increasing importance for material science and engineering in the future.

Acknowledgements

The authors wish to acknowledge the financial support from the Australian Research Council (FT130101094).

Conflict of Interest

The authors declare no conflict of interest.

Keywords

metamaterials, phononic crystals, photonic crystals, topology optimization

Received: January 26, 2019
Revised: March 23, 2019
Published online: April 26, 2019

[1] L. Rayleigh, *London, Edinburgh, Dublin Philos. Mag. J. Sci.* **1887**, *24*, 145.
[2] S. John, *Phys. Rev. Lett.* **1987**, *58*, 2486.
[3] E. Yablonovitch, *Phys. Rev. Lett.* **1987**, *58*, 2059.
[4] M. Sigalas, E. N. Economou, *Solid State Commun.* **1993**, *86*, 141.
[5] M. S. Kushwaha, P. Halevi, L. Dobrzynski, R. Djafari, *Phys. Rev. Lett.* **1993**, *71*, 2022.
[6] J. C. Knight, T. A. Birks, P. S. J. Russell, D. M. Atkin, *Opt. Lett.* **1996**, *21*, 1547.
[7] B. Temelkuran, S. D. Hart, G. Benoit, J. D. Joannopoulos, Y. Fink, *Nature* **2002**, *420*, 650.
[8] S. A. Rinne, F. García-Santamaría, P. V. Braun, *Nat. Photonics* **2008**, *2*, 52.
[9] D. Richards, D. J. Pines, *J. Sound Vib.* **2003**, *264*, 317.
[10] M. M. Sigalas, *J. Appl. Phys.* **1998**, *84*, 3026.
[11] M. Kafesaki, M. M. Sigalas, N. García, *Phys. Rev. Lett.* **2000**, *85*, 4044.
[12] A. Khelif, A. Choujaa, S. Benchabane, B. Djafari-Rouhani, V. Laude, *Appl. Phys. Lett.* **2004**, *84*, 4400.
[13] D. R. Smith, W. J. Padilla, D. C. Vier, S. C. Nemat-Nasser, S. Schultz, *Phys. Rev. Lett.* **2000**, *84*, 4184.
[14] V. G. Veselago, *Phys.-Usp.* **1968**, *10*, 509.
[15] J. B. Pendry, A. J. Holden, D. J. Robbins, W. J. Stewart, *IEEE Trans. Microwave Theory Tech.* **1999**, *47*, 2075.
[16] R. A. Shelby, D. R. Smith, S. Schultz, *Science* **2001**, *292*, 77.
[17] Y. Ding, Z. Liu, C. Qiu, J. Shi, *Phys. Rev. Lett.* **2007**, *99*, 093904.
[18] Y. Wu, Y. Lai, Z. Zhang, *Phys. Rev. Lett.* **2011**, *107*, 105506.
[19] X. N. Liu, G. K. Hu, G. L. Huang, C. T. Sun, *Appl. Phys. Lett.* **2011**, *98*, 251907.
[20] Y. Chen, G. Hu, G. Huang, *J. Mech. Phys. Solids* **2017**, *105*, 179.
[21] Y. Lai, Y. Wu, P. Sheng, Z.-Q. Zhang, *Nat. Mater.* **2011**, *10*, 620.
[22] C. M. Park, J. J. Park, S. H. Lee, Y. M. Seo, C. K. Kim, S. H. Lee, *Phys. Rev. Lett.* **2011**, *107*, 194301.
[23] N. Kaina, F. Lemoult, M. Fink, G. Lerosey, *Nature* **2015**, *525*, 77.
[24] M. P. Bendsøe, N. Kikuchi, *Comput. Methods Appl. Mech. Eng.* **1988**, *71*, 197.
[25] M. P. Bendsøe, *Struct. Optim.* **1989**, *1*, 193.
[26] G. I. N. Rozvany, *Structural Design via Optimality Criteria*, Kluwer Academic Publishers Group, London **1989**.
[27] M. Zhou, G. I. N. Rozvany, *Comput. Methods Appl. Mech. Eng.* **1991**, *89*, 309.
[28] G. Allaire, F. Jouve, A.-M. Toader, *J. Comput. Phys.* **2004**, *194*, 363.
[29] M. Y. Wang, X. Wang, D. Guo, *Comput. Methods Appl. Mech. Eng.* **2003**, *192*, 227.
[30] G. Allaire, F. Jouve, A.-M. Toader, *C. R. Seances Acad. Sci., Ser. A* **2002**, 1125.
[31] X. Huang, Y. M. Xie, *Finite Elem. Anal. Des.* **2007**, *43*, 1039.
[32] X. Huang, Y. M. Xie, *Comput. Mech.* **2009**, *43*, 393.
[33] J. H. Holland, *Q. Rev. Biol.* **1975**, *6*, 126.
[34] D. E. Goldberg, J. H. Holland, *Mach. Learn.* **1988**, *3*, 95.

© 2019 WILEY-VCH Verlag GmbH & Co. KGaA, Weinheim

25130390, 2019, 7, Downloaded from https://onlinelibrary.wiley.com/doi/10.1002/adts.201900017 by The Librarian, Wiley Online Library on [03/06/2024]. See the Terms and Conditions (https://onlinelibrary.wiley.com/terms-and-conditions) on Wiley Online Library for rules of use; OA articles are governed by the applicable Creative Commons License

[35] D. Goldberg, *Genetic Algorithms in Search, Optimization, and Machine Learning*, Addison-Wesley Professional, Reading, MA **1989**.
[36] G. I. N. Rozvany, *Struct. Multidiscipl. Optim.* **2009**, *37*, 217.
[37] O. Sigmund, K. Maute, *Struct. Multidiscipl. Optim.* **2013**, *48*, 1031.
[38] J. E. Cadman, S. Zhou, Y. Chen, Q. Li, *J. Mater. Sci.* **2013**, *48*, 51.
[39] J. S. Jensen, O. Sigmund, *Laser Photonics Rev.* **2011**, *5*, 308.
[40] S. Molesky, Z. Lin, A. Y. Piggott, W. Jin, J. Vucković, A. W. Rodriguez, *Nat. Photonics* **2018**, *12*, 659.
[41] M.-H. Lu, L. Feng, Y.-F. Chen, *Mater. Today* **2009**, *12*, 34.
[42] M. I. Hussein, M. J. Leamy, M. Ruzzene, *Appl. Mech. Rev.* **2014**, *66*, 040802.
[43] G. Yi, B. Youn, *Struct. Multidiscipl. Optim.* **2016**, *54*, 1315.
[44] S. Fan, P. R. Villeneuve, J. D. Joannopoulos, E. F. Schubert, *Phys. Rev. Lett.* **1997**, *78*, 3294.
[45] A. D. Falco, L. O'Faolain, T. F. Krauss, *Appl. Phys. Lett.* **2009**, *94*, 063503.
[46] Y. Akahane, T. Asano, B.-S. Song, S. Noda, *Nature* **2003**, *425*, 944.
[47] B.-S. Song, S. Noda, T. Asano, *Science* **2003**, *300*, 1537.
[48] B.-S. Song, S. Noda, T. Asano, Y. Akahane, *Nat. Mater.* **2005**, *4*, 207.
[49] S. Noda, M. Fujita, T. Asano, *Nat. Photonics* **2007**, *1*, 449.
[50] M. G. Scullion, A. Di Falco, T. F. Krauss, *Biosens. Bioelectron.* **2011**, *27*, 101.
[51] L. A. Woldering, A. P. Mosk, W. L. Vos, *Phys. Rev. B* **2014**, *90*, 115140.
[52] S. Hu, S. M. Weiss, *ACS Photonics* **2016**, *3*, 1647.
[53] T. A. Birks, J. C. Knight, P. S. J. Russell, *Opt. Lett.* **1997**, *22*, 961.
[54] R. F. Cregan, B. J. Mangan, J. C. Knight, T. A. Birks, P. S. J. Russell, P. J. Roberts, D. C. Allan, *Science* **1999**, *285*, 1537.
[55] J. C. Knight, *Nature* **2003**, *424*, 847.
[56] W. J. Wadsworth, R. M. Percival, G. Bouwmans, J. C. Knight, P. S. J. Russell, *Opt. Express* **2003**, *11*, 48.
[57] F. Du, Y.-Q. Lu, S.-T. Wu, *Appl. Phys. Lett.* **2004**, *85*, 2181.
[58] J. H. Lim, K. S. Lee, J. C. Kim, B. H. Lee, *Opt. Lett.* **2004**, *29*, 331.
[59] M. W. Haakestad, T. T. Alkeskjold, M. D. Nielsen, L. Scolari, J. Riishede, H. E. Engan, A. Bjarklev, *IEEE Photonics Technol. Lett.* **2005**, *17*, 819.
[60] J. Villatoro, V. Finazzi, V. P. Minkovich, V. Pruneri, G. Badenes, *Appl. Phys. Lett.* **2007**, *91*, 091109.
[61] D. K. C. Wu, B. T. Kuhlmey, B. J. Eggleton, *Opt. Lett.* **2009**, *34*, 322.
[62] A. M. R. Pinto, M. Lopez-Amo, *J. Sens.* **2012**, *2012*, 1.
[63] C. Jauregui, J. Limpert, A. Tünnermann, *Nat. Photonics* **2013**, *7*, 861.
[64] A. Mekis, J. C. Chen, I. Kurland, S. Fan, P. R. Villeneuve, J. D. Joannopoulos, *Phys. Rev. Lett.* **1996**, *77*, 3787.
[65] S.-Y. Lin, E. Chow, V. Hietala, P. R. Villeneuve, J. D. Joannopoulos, *Science* **1998**, *282*, 274.
[66] M. Bayindir, B. Temelkuran, E. Ozbay, *Appl. Phys. Lett.* **2000**, *77*, 3902.
[67] A. Chutinan, S. John, O. Toader, *Phys. Rev. Lett.* **2003**, *90*, 123901.
[68] S. Kim, G. P. Nordin, J. Cai, J. Jiang, *Opt. Lett.* **2003**, *28*, 2384.
[69] S. J. McNab, N. Moll, Y. A. Vlasov, *Opt. Express* **2003**, *11*, 2927.
[70] C.-C. Chen, H.-D. Chien, P.-G. Luan, *Appl. Opt.* **2004**, *43*, 6187.
[71] E. Schonbrun, Q. Wu, W. Park, T. Yamashita, C. J. Summers, *Opt. Lett.* **2006**, *31*, 3104.
[72] D. M. Beggs, T. P. White, L. O'Faolain, T. F. Krauss, *Opt. Lett.* **2008**, *33*, 147.
[73] W.-C. Lai, S. Chakravarty, X. Wang, C. Lin, R. T. Chen, *Opt. Lett.* **2011**, *36*, 984.
[74] X. Gao, J. H. Shi, X. Shen, H. F. Ma, W. X. Jiang, L. Li, T. J. Cui, *Appl. Phys. Lett.* **2013**, *102*, 151912.
[75] J. B. Pendry, *Phys. Rev. Lett.* **2000**, *85*, 3966.
[76] C. Luo, S. G. Johnson, J. D. Joannopoulos, J. B. Pendry, *Phys. Rev. B* **2002**, *65*, 201104.
[77] L. Maigyte, V. Purlys, J. Trull, M. Peckus, C. Cojocaru, D. Gailevičius, M. Malinauskas, K. Staliunas, *Opt. Lett.* **2013**, *38*, 2376.
[78] M. Notomi, *Phys. Rev. B* **2000**, *62*, 10696.
[79] P. V. Parimi, W. T. Lu, P. Vodo, S. Sridhar, *Nature* **2003**, *426*, 404.
[80] E. Cubukcu, K. Aydin, E. Ozbay, S. Foteinopoulou, C. M. Soukoulis, *Nature* **2003**, *423*, 604.
[81] J. D. Joannopoulos, S. G. Johnson, J. N. Winn, R. D. Mead, *Photonic Crystals: Molding the Flow of Light*, Princeton University Press, Princeton **2011**.
[82] H. Kosaka, T. Kawashima, A. Tomita, M. Notomi, T. Tamamura, T. Sato, S. Kawakami, *Phys. Rev. B* **1998**, *58*, R10096.
[83] W. Lijun, M. Mazilu, T. Karle, T. F. Krauss, *IEEE J. Quantum Electron.* **2002**, *38*, 915.
[84] C. Luo, M. Soljačić, J. D. Joannopoulos, *Opt. Lett.* **2004**, *29*, 745.
[85] T. Matsumoto, K.-S. Eom, T. Baba, *Opt. Lett.* **2006**, *31*, 2786.
[86] C. Luo, S. G. Johnson, J. D. Joannopoulos, J. B. Pendry, *Phys. Rev. B* **2003**, *68*, 045115.
[87] M. Doosje, B. J. Hoenders, J. Knoester, *J. Opt. Soc. Am. B* **2000**, *17*, 600.
[88] H. Kurt, M. Turduev, I. H. Giden, *Opt. Express* **2012**, *20*, 7184.
[89] P. Shi, K. Huang, Y.-p. Li, *Opt. Commun.* **2012**, *285*, 3128.
[90] Y.-F. Chau, F.-L. Wu, Z.-H. Jiang, H.-Y. Li, *Opt. Express* **2011**, *19*, 4862.
[91] O. R. Bilal, M. I. Hussein, in *Photonic and Phononic Properties of Engineered Nanostructures II*, Vol. 8269 (Eds: A. Adibi, S. Y. Lin, A. Scherer), SPIE, Bellingham, WA**2012**.
[92] F. Meng, X. Huang, B. Jia, *J. Comput. Phys.* **2015**, *302*, 393.
[93] W. Axmann, P. Kuchment, *J. Comput. Phys.* **1999**, *150*, 468.
[94] H.-W. Dong, Y.-S. Wang, Y.-F. Wang, C. Zhang, *AIP Adv.* **2015**, *5*, 117149.
[95] Y. Li, X. Huang, F. Meng, S. Zhou, *Struct. Multidiscipl. Optim.* **2016**, *54*, 595.
[96] S. Guo, S. Albin, *Opt. Express* **2003**, *11*, 167.
[97] S. Shi, C. Chen, D. W. Prather, *J. Opt. Soc. Am. A* **2004**, *21*, 1769.
[98] Y. Kane, *IEEE Trans. Antennas Propag.* **1966**, *14*, 302.
[99] S. Guo, F. Wu, S. Albin, R. S. Rogowski, *Opt. Express* **2004**, *12*, 1741.
[100] J.-H. Sun, T.-T. Wu, *Phys. Rev. B* **2007**, *76*, 104304.
[101] L. Oyhenart, V. Vigneras, in *Photonic Crystals: Introduction, Applications and Theory* (Ed: A. Massaro), IntechOpen, London **2012**, p. 267.
[102] S. J. Cox, D. C. Dobson, *SIAM J. Appl. Math.* **1999**, *59*, 2108.
[103] S. J. Cox, D. C. Dobson, *J. Comput. Phys.* **2000**, *158*, 214.
[104] C. Y. Kao, S. Osher, E. Yablonovitch, *Appl. Phys. B* **2005**, *81*, 235.
[105] L. He, C.-Y. Kao, S. Osher, *J. Comput. Phys.* **2007**, *225*, 891.
[106] O. Sigmund, K. Hougaard, *Phys. Rev. Lett.* **2008**, *100*, 153904.
[107] H. Men, N. C. Nguyen, R. M. Freund, P. A. Parrilo, J. Peraire, *J. Comput. Phys.* **2010**, *229*, 3706.
[108] H. Men, N. C. Nguyen, R. M. Freund, K. M. Lim, P. A. Parrilo, J. Peraire, *Phys. Rev. E* **2011**, *83*, 046703.
[109] A. Takezawa, M. Kitamura, *J. Comput. Phys.* **2014**, *257*, 216.
[110] X.-l. Cheng, J. Yang, *J Opt. Soc. Am. A* **2013**, *30*, 2314.
[111] J. Goh, I. Fushman, D. Englund, J. Vučković, *Opt. Express* **2007**, *15*, 8218.
[112] J. S. Jensen, O. Sigmund, *Appl. Phys. Lett.* **2004**, *84*, 2022.
[113] M. P. Bendsøe, O. Sigmund, *Ing.-Arch.* **1999**, *69*, 635.
[114] F. Meng, Y. Li, S. Li, H. Lin, B. Jia, X. Huang, *J. Lightwave Technol.* **2017**, *35*, 1670.
[115] E. Lidorikis, M. M. Sigalas, E. N. Economou, C. M. Soukoulis, *Phys. Rev. B* **2000**, *61*, 13458.
[116] L. Shen, Z. Ye, S. He, *Phys. Rev. B* **2003**, *68*, 035109.
[117] D. Wang, Z. Yu, Y. Liu, P. Lu, L. Han, H. Feng, X. Guo, H. Ye, *Opt. Express* **2011**, *19*, 19346.
[118] F. Meng, S. Li, Y. F. Li, B. Jia, X. Huang, *Mater. Lett.* **2017**, *207*, 176.
[119] Y. Chen, F. Meng, G. Li, X. Huang, *Smart Mater. Struct.* **2018**, *28*.
[120] M. Botey, Y.-C. Cheng, V. Romero-Garcia, R. Picó, R. Herrero, V. Sánchez-Morcillo, K. Staliunas, *Opt. Lett.* **2013**, *38*, 1890.
[121] K. M. Ho, C. T. Chan, C. M. Soukoulis, *Phys. Rev. Lett.* **1990**, *65*, 3152.

© 2019 WILEY-VCH Verlag GmbH & Co. KGaA, Weinheim

25130390, 2019, 7, Downloaded from https://onlinelibrary.wiley.com/doi/10.1002/adts.201900017 by The Librarian, Wiley Online Library on [03/06/2024]. See the Terms and Conditions (https://onlinelibrary.wiley.com/terms-and-conditions) on Wiley Online Library for rules of use; OA articles are governed by the applicable Creative Commons License

[122] M. Maldovan, E. L. Thomas, C. W. Carter, *Appl. Phys. Lett.* **2004**, 84, 362.
[123] N. Vasilantonakis, K. Terzaki, I. Sakellari, V. Purlys, D. Gray, C. M. Soukoulis, M. Vamvakaki, M. Kafesaki, M. Farsari, *Adv. Mater.* **2012**, *24*, 1101.
[124] S. Fan, P. R. Villeneuve, R. D. Meade, J. D. Joannopoulos, *Appl. Phys. Lett.* **1994**, *65*, 1466.
[125] S. G. Johnson, J. D. Joannopoulos, *Appl. Phys. Lett.* **2000**, *77*, 3490.
[126] A. Chutinan, S. Noda, *Phys. Rev. B* **1998**, *57*, R2006.
[127] P. Sun, J. D. Williams, *IEEE Photonics J.* **2012**, *4*, 1155.
[128] H. Men, K. Y. K. Lee, R. M. Freund, J. Peraire, S. G. Johnson, *Opt. Express* **2014**, *22*, 22632.
[129] F. Meng, B. Jia, X. Huang, *Adv. Theory Simul.* **2018**, *1*, 1800122.
[130] F. Meng, S. Li, H. Lin, B. Jia, X. Huang, *Finite Elem. Anal. Des.* **2016**, *117-118*, 46.
[131] S. Li, F. Meng, H. Lin, X. Huang, B. Jia, *Photonics Nanostruct.* **2017**, *27*, 11.
[132] G. T. Reed, *Silicon Photonics: The State of the Art*, John Wiley & Sons, West Sussex **2008**.
[133] F. Wang, J. S. Jensen, O. Sigmund, *J. Opt. Soc. Am. B* **2011**, *28*, 387.
[134] P. I. Borel, A. Harpøth, L. H. Frandsen, M. Kristensen, P. Shi, J. S. Jensen, O. Sigmund, *Opt. Express* **2004**, *12*, 1996.
[135] L. Yang, A. V. Lavrinenko, L. H. Frandsen, P. I. Borel, A. Tetu, J. F. Pedersen, *Electron. Lett.* **2007**, *43*, 923.
[136] L. Yang, A. V. Lavrinenko, J. M. Hvam, O. Sigmund, *Appl. Phys. Lett.* **2009**, *95*, 261101.
[137] A. Y. Piggott, J. Petykiewicz, L. Su, J. Vučković, *Sci. Rep.* **2017**, *7*, 1786.
[138] L. Su, A. Y. Piggott, N. V. Sapra, J. Petykiewicz, J. Vučković, *ACS Photonics* **2018**, *5*, 301.
[139] X. Liang, S. G. Johnson, *Opt. Express* **2013**, *21*, 30812.
[140] F. Wang, R. E. Christiansen, Y. Yu, J. Mørk, O. Sigmund, *Appl. Phys. Lett.* **2018**, *113*, 241101.
[141] C. Dory, D. Vercruysse, K. Y. Yang, N. V. Sapra, A. E. Rugar, S. Sun, D. M. Lukin, A. Y. Piggott, J. L. Zhang, M. Radulaski, K. G. Lagoudakis, L. Su, J. Vuckovic, arXiv:1812.02287, **2018**.
[142] B. Khanaliloo, M. Mitchell, A. C. Hryciw, P. E. Barclay, *Nano Lett.* **2015**, *15*, 5131.
[143] H. J. Kimble, *Nature* **2008**, *453*, 1023.
[144] B. C. Rose, D. Huang, Z.-H. Zhang, P. Stevenson, A. M. Tyryshkin, S. Sangtawesin, S. Srinivasan, L. Loudin, M. L. Markham, A. M. Edmonds, D. J. Twitchen, S. A. Lyon, N. P. de Leon, *Science* **2018**, *361*, 60.
[145] F. Callewaert, V. Velev, S. Jiang, A. V. Sahakian, P. Kumar, K. Aydin, *Appl. Phys. Lett.* **2018**, *112*, 091102.
[146] M. Sigalas, S. Kushwaha Manvir, N. Economou Eleftherios, M. Kafesaki, E. Psarobas Ioannis, W. Steurer, *Zeitschrift für Kristallographie—Crystalline Materials*, Vol. *220*, **2005**, p. 765.
[147] C. Croënne, E. J. S. Lee, H. Hu, J. H. Page, *AIP Adv.* **2011**, *1*, 041401.
[148] J. V. Sanchez-Perez, C. Rubio, R. Martinez-Sala, R. Sanchez-Grandia, V. Gomez, *Appl. Phys. Lett.* **2002**, *81*, 5240.
[149] I. R. H. Olsson, I. El-Kady, *Meas. Sci. Technol.* **2009**, *20*, 012002.
[150] O. Oralkan, A. S. Ergun, J. A. Johnson, M. Karaman, U. Demirci, K. Kaviani, T. H. Lee, B. T. Khuri-Yakub, *IEEE Trans. Ultrason., Ferroelectr. Freq. Control* **2002**, *49*, 1596.
[151] Y. Aichao, L. Ping, W. Yumei, Y. Chao, W. Decai, Z. Feng, Z. Jiajia, *Appl. Phys. Express* **2015**, *8*, 057101.
[152] S. Mohammadi, A. A. Eftekhar, W. D. Hunt, A. Adibi, *Appl. Phys. Lett.* **2009**, *94*, 051906.
[153] P. H. Otsuka, K. Nanri, O. Matsuda, M. Tomoda, D. M. Profunser, I. A. Veres, S. Danworaphong, A. Khelif, S. Benchabane, V. Laude, O. B. Wright, *Sci. Rep.* **2013**, *3*, 3351.
[154] Y. Pennec, J. O. Vasseur, B. Djafari-Rouhani, L. Dobrzyński, P. A. Deymier, *Surf. Sci. Rep.* **2010**, *65*, 229.
[155] H. Policarpo, M. M. Neves, A. M. R. Ribeiro, *Shock Vib.* **2010**, *17*, 521.
[156] A. Khelif, S. Mohammadi, A. A. Eftekhar, A. Adibi, B. Aoubiza, *J. Appl. Phys.* **2010**, *108*, 084515.
[157] A. Khelif, P. A. Deymier, B. Djafari-Rouhani, J. O. Vasseur, L. Dobrzynski, *J. Appl. Phys.* **2003**, *94*, 1308.
[158] I. El-Kady, R. H. O. III, J. G. Fleming, *Appl. Phys. Lett.* **2008**, *92*, 233504.
[159] O. Umnova, K. Attenborough, C. M. Linton, *J. Acoust. Soc. Am.* **2006**, *119*, 278.
[160] J. Sánchez-Dehesa, V. M. Garcia-Chocano, D. Torrent, F. Cervera, S. Cabrera, F. Simon, *J. Acoust. Soc. Am.* **2011**, *129*, 1173.
[161] X. Zhang, Z. Liu, *Appl. Phys. Lett.* **2004**, *85*, 341.
[162] D. Zhao, Y. Ye, S. Xu, X. Zhu, L. Yi, *Appl. Phys. Lett.* **2014**, *104*, 043503.
[163] S. Yang, J. H. Page, Z. Liu, M. L. Cowan, C. T. Chan, P. Sheng, *Phys. Rev. Lett.* **2004**, *93*, 024301.
[164] M. Ke, Z. Liu, C. Qiu, W. Wang, J. Shi, W. Wen, P. Sheng, *Phys. Rev. B* **2005**, *72*, 064306.
[165] A. Sukhovich, B. Merheb, K. Muralidharan, J. O. Vasseur, Y. Pennec, P. A. Deymier, J. H. Page, *Phys. Rev. Lett.* **2009**, *102*, 154301.
[166] L. Feng, X.-P. Liu, M.-H. Lu, Y.-B. Chen, Y.-F. Chen, Y.-W. Mao, J. Zi, Y.-Y. Zhu, S.-N. Zhu, N.-B. Ming, *Phys. Rev. Lett.* **2006**, *96*, 014301.
[167] O. Sigmund, J. S. Jensen, *Philos. Trans. R. Soc., A* **2003**, *361*, 1001.
[168] A. P. Seyranian, E. Lund, N. Olhoff, *Struct. Optim.* **1994**, *8*, 207.
[169] J. S. Jensen, N. L. Pedersen, *J. Sound Vib.* **2006**, *289*, 967.
[170] J. Du, N. Olhoff, *Struct. Multidiscipl. Optim.* **2007**, *34*, 91.
[171] G. A. Gazonas, D. S. Weile, R. Wildman, A. Mohan, *Int. J. Solids Struct.* **2006**, *43*, 5851.
[172] M. I. Hussein, K. Hamza, G. M. Hulbert, K. Saitou, *Wave Random Complex* **2007**, *17*, 491.
[173] O. R. Bilal, M. I. Hussein, *Phy. Rev. E* **2011**, *84*, 065701.
[174] D. Hao-Wen, S. Xiao-Xing, W. Yue-Sheng, *J. Phys. D: Appl. Phys.* **2014**, *47*, 155301.
[175] K. Deb, A. Pratap, S. Agarwal, T. Meyarivan, *IEEE Trans. Evol. Comput.* **2002**, *6*, 182.
[176] J. M. Herrero, S. García-Nieto, X. Blasco, V. Romero-García, J. V. Sánchez-Pérez, L. M. Garcia-Raffi, *Struct. Multidiscipl. Optim.* **2009**, *39*, 203.
[177] Y. Li, X. Huang, S. Zhou, *Materials* **2016**, *9*, 186.
[178] Z. Zhang, Y. Li, F. Meng, X. Huang, *Comput. Mater. Sci.* **2017**, *139*, 97.
[179] Y. Li, F. Meng, S. Li, B. Jia, S. Zhou, X. Huang, *Phys. Lett. A* **2018**, *382*, 679.
[180] Y. Chen, F. Meng, G. Sun, G. Li, X. Huang, *J. Sound Vib.* **2017**, *410*, 103.
[181] J. He, Z. Kang, *Ultrasonics* **2018**, *82*, 1.
[182] Y. Lu, Y. Yang, J. K. Guest, A. Srivastava, *Sci. Rep.* **2017**, *7*, 43407.
[183] W. Li, F. Meng, Y. Li, X. Huang, unpublished.
[184] J. H. Oh, Y. J. Kim, Y. Y. Kim, *J. Appl. Phys.* **2013**, *113*, 106101.
[185] A. O. Krushynska, V. G. Kouznetsova, M. G. D. Geers, *J. Mech. Phys. Solids* **2016**, *96*, 29.
[186] H. Al Ba'ba'a, M. Nouh, *J. Vib. Acoust.* **2017**, *139*, 021003.
[187] E. Andreassen, J. S. Jensen, *Struct. Multidiscipl. Optim.* **2014**, *49*, 695.
[188] Y. Chen, D. Guo, Y. F. Li, G. Li, X. Huang, *Ultrasonics* **2019**, *94*, 419.
[189] E. Andreassen, J. S. Jensen, *J. Vib. Acoust.* **2013**, *135*, 041015.
[190] W. Zhang, Z. Kang, *Int. J. Numer. Methods Eng.* **2017**, *110*, 31.
[191] X. Zhang, J. He, A. Takezawa, Z. Kang, *Int. J. Numer. Methods Eng.* **2018**, *115*, 1154.
[192] X. Zhang, A. Takezawa, Z. Kang, *Comput. Mater. Sci.* **2019**, *160*, 159.
[193] L. Xie, B. Xia, G. Huang, J. Lei, J. Liu, *Struct. Multidiscipl. Optim.* **2017**, *56*, 1319.
[194] L. Xie, J. Liu, G. Huang, W. Zhu, B. Xia, *Int. J. Numer. Methods Eng.* **2018**, *114*, 777.
[195] Y. F. Li, F. Meng, S. Zhou, M.-H. Lu, X. Huang, *Sci. Rep.* **2017**, *7*.

© 2019 WILEY-VCH Verlag GmbH & Co. KGaA, Weinheim

25130390, 2019, 7, Downloaded from https://onlinelibrary.wiley.com/doi/10.1002/adts.201900017 by The Librarian, Wiley Online Library on [03/06/2024]. See the Terms and Conditions (https://onlinelibrary.wiley.com/terms-and-conditions) on Wiley Online Library for rules of use; OA articles are governed by the applicable Creative Commons License

[196] S. Halkjær, O. Sigmund, J. S. Jensen, *Struct. Multidiscipl. Optim.* **2006**, *32*, 263.
[197] T. Borrvall, J. Petersson, *Comput. Method. Appl. Mech. Eng.* **2001**, *190*, 4911.
[198] S. Hedayatrasa, K. Abhary, M. Uddin, C.-T. Ng, *J. Mech. Phys. Solids* **2016**, *89*, 31.
[199] S. Hedayatrasa, M. Kersemans, K. Abhary, M. Uddin, J. K. Guest, W. Van Paepegem, *Mech. Mater.* **2017**, *105*, 188.
[200] C. Rupp, A. Evgrafov, K. Maute, M. Dunn, *Struct. Multidiscipl. Optim.* **2007**, *34*, 111.
[201] K. Svanberg, *Struct. Multidiscip. Optim.* **1987**, *42*, 665.
[202] C. J. Rupp, M. L. Dunn, K. Maute, *Appl. Phys. Lett.* **2010**, *96*, 111902.
[203] R. W. Ziolkowski, N. Engheta, *Metamaterials: Physics and Engineering Explorations*, John Wiley & Sons, New York **2006**.
[204] D. R. Smith, J. B. Pendry, M. C. K. Wiltshire, *Science* **2004**, *305*, 788.
[205] J. Yao, Z. Liu, Y. Liu, Y. Wang, C. Sun, G. Bartal, A. M. Stacy, X. Zhang, *Science* **2008**, *321*, 930.
[206] W. J. Padilla, D. N. Basov, D. R. Smith, *Mater. Today* **2006**, *9*, 28.
[207] R. W. Ziolkowski, E. Heyman, *Phys. Rev. E* **2001**, *64*, 056625.
[208] A. Poddubny, I. Iorsh, P. Belov, Y. Kivshar, *Nat. Photonics* **2013**, *7*, 948.
[209] C. M. Soukoulis, M. Wegener, *Nat. Photonics* **2011**, *5*, 523.
[210] S. Foteinopoulou, *Phys. B* **2012**, *407*, 4056.
[211] M. V. Rybin, D. S. Filonov, K. B. Samusev, P. A. Belov, Y. S. Kivshar, M. F. Limonov, *Nat. Commun.* **2015**, *6*, 10102.
[212] J. B. Pendry, A. J. Holden, W. J. Stewart, I. Youngs, *Phys. Rev. Lett.* **1996**, *76*, 4773.
[213] D. Schurig, J. J. Mock, D. R. Smith, *Appl. Phys. Lett.* **2006**, *88*, 041109.
[214] A. Demetriadou, J. B. Pendry, *J. Phys.: Condens. Matter* **2008**, *20*, 295222.
[215] W. J. Padilla, M. T. Aronsson, C. Highstrete, M. Lee, A. J. Taylor, R. D. Averitt, *Phys. Rev. B* **2007**, *75*, 041102.
[216] M. C. K. Wiltshire, J. B. Pendry, J. V. Hajnal, *J. Phys.: Condens. Matter* **2009**, *21*, 292201.
[217] C. Rockstuhl, C. Menzel, T. Paul, T. Pertsch, F. Lederer, *Phys. Rev. B* **2008**, *78*, 155102.
[218] J. Valentine, S. Zhang, T. Zentgraf, E. Ulin-Avila, D. A. Genov, G. Bartal, X. Zhang, *Nature* **2008**, *455*, 376.
[219] P. Moitra, Y. Yang, Z. Anderson, I. I. Kravchenko, D. P. Briggs, J. Valentine, *Nat. Photonics* **2013**, *7*, 791.
[220] K. C. Huang, M. L. Povinelli, J. D. Joannopoulos, *Appl. Phys. Lett.* **2004**, *85*, 543.
[221] C. Wu, A. B. Khanikaev, G. Shvets, *Phys. Rev. Lett.* **2011**, *106*, 107403.
[222] A. Alu, N. Engheta, *IEEE Trans. Microwave Theory Tech.* **2004**, *52*, 199.
[223] Z. Liu, N. Fang, T.-J. Yen, X. Zhang, *Appl. Phys. Lett.* **2003**, *83*, 5184.
[224] X. Zhang, Z. Liu, *Nat. Mater.* **2008**, *7*, 435.
[225] H. Tao, N. I. Landy, C. M. Bingham, X. Zhang, R. D. Averitt, W. J. Padilla, *Opt. Express* **2008**, *16*, 7181.
[226] H. Tao, C. M. Bingham, A. C. Strikwerda, D. Pilon, D. Shrekenhamer, N. I. Landy, K. Fan, X. Zhang, W. J. Padilla, R. D. Averitt, *Phys. Rev. B* **2008**, *78*, 241103.
[227] N. I. Landy, S. Sajuyigbe, J. J. Mock, D. R. Smith, W. J. Padilla, *Phys. Rev. Lett.* **2008**, *100*, 207402.
[228] M. Tonouchi, *Nat. Photonics* **2007**, *1*, 97.
[229] P. W. Gwyn, *Rep. Prog. Phys.* **2006**, *69*, 301.
[230] J. Li, J. B. Pendry, *Phys. Rev. Lett.* **2008**, *101*, 203901.
[231] W. Cai, U. K. Chettiar, A. V. Kildishev, V. M. Shalaev, *Nat. Photonics* **2007**, *1*, 224.
[232] F. Zolla, S. Guenneau, A. Nicolet, J. B. Pendry, *Opt. Lett.* **2007**, *32*, 1069.
[233] J. B. Pendry, D. Schurig, D. R. Smith, *Science* **2006**, *312*, 1780.
[234] A. Alu, N. Engheta, *IEEE Trans. Antennas Propag.* **2003**, *51*, 2558.
[235] A. Alù, N. Engheta, *Phys. Rev. E* **2005**, *72*, 016623.
[236] H. F. Ma, T. J. Cui, *Nat. Commun.* **2010**, *1*, 21.
[237] R. Liu, C. Ji, J. J. Mock, J. Y. Chin, T. J. Cui, D. R. Smith, *Science* **2009**, *323*, 366.
[238] P.-Y. Chen, A. Alù, *ACS Nano* **2011**, *5*, 5855.
[239] A. R. Diaz, O. Sigmund, *Struct. Multidiscipl. Optim.* **2010**, *41*, 163.
[240] D. R. Smith, D. C. Vier, T. Koschny, C. M. Soukoulis, *Phys. Rev. E* **2005**, *71*, 036617.
[241] O. Sigmund, in *IUTAM Symposium on Modelling Nanomaterials and Nanosystems* (Eds: R. Pyrz, J. C. Rauhe), Dordrecht, Netherlands **2009**.
[242] M. Otomori, T. Yamada, K. Izui, S. Nishiwaki, J. Andkjær, *Comput. Method Appl. Mech. Eng.* **2012**, *237–240*, 192.
[243] D. R. Smith, J. B. Pendry, *J. Opt. Soc. Am. B* **2006**, *23*, 391.
[244] D. R. Smith, S. Schultz, P. Markoš, C. M. Soukoulis, *Phys. Rev. B* **2002**, *65*, 195104.
[245] O. Ouchetto, C. Qiu, S. Zouhdi, L. Li, A. Razek, *IEEE Trans. Microwave Theory Tech.* **2006**, *54*, 3893.
[246] X. Chen, T. M. Grzegorczyk, B.-I. Wu, J. Pacheco, J. A. Kong, *Phys. Rev. E* **2004**, *70*, 016608.
[247] S. Zhou, W. Li, Y. Chen, G. Sun, Q. Li, *Acta Mater.* **2011**, *59*, 2624.
[248] S. Zhou, W. Li, G. Sun, Q. Li, *Opt. Express* **2010**, *18*, 6693.
[249] R. F. Harrington, *Field Computation by Moment Methods*, Wiley-IEEE Press, New York **1993**.
[250] J. M. Jin, The Finite Element Method in Electromagnetics, John Wiley & Sons, New York **1993**.
[251] M. Otomori, T. Yamada, J. Andkjær, K. Izui, S. Nishiwaki, N. Kogiso, *IEEE Trans. Magn.* **2013**, *49*, 2081.
[252] M. Otomori, T. Yamada, K. Izui, S. Nishiwaki, J. Andkjær, *Struct. Multidiscipl. Optim.* **2017**, *55*, 913.
[253] Z. Hashin, *J. Appl. Mech.* **1983**, *50*, 481.
[254] O. Sigmund, *Int. J. Solids Struct.* **1994**, *31*, 2313.
[255] P. Cheben, R. Halir, J. H. Schmid, H. A. Atwater, D. R. Smith, *Nature* **2018**, *560*, 565.
[256] Z. Yu, H. Cui, X. Sun, *Opt. Lett.* **2017**, *42*, 3093.
[257] B. Shen, P. Wang, R. Polson, R. Menon, *Nat. Photonics* **2015**, *9*, 378.
[258] B. Shen, P. Wang, R. Polson, R. Menon, *Opt. Express* **2014**, *22*, 27175.
[259] B. Shen, P. Wang, R. Polson, R. Menon, *Optica* **2014**, *1*, 356.
[260] P. Wang, R. Menon, *Opt. Express* **2014**, *22*, A99.
[261] L. Lu, D. Liu, F. Zhou, D. Li, M. Cheng, L. Deng, S. Fu, J. Xia, M. Zhang, *Opt. Lett.* **2016**, *41*, 5051.
[262] X. Zhang, *Phys. Rev. Lett.* **2008**, *100*, 113903.
[263] X. Huang, Y. Lai, Z. H. Hang, H. Zheng, C. T. Chan, *Nat. Mater.* **2011**, *10*, 582.
[264] I. Liberal, N. Engheta, *Nat. Photonics* **2017**, *11*, 149.
[265] Y. Li, S. Kita, P. Muñoz, O. Reshef, D. I. Vulis, M. Yin, M. Lončar, E. Mazur, *Nat. Photonics* **2015**, *9*, 738.
[266] S. Raghu, F. D. M. Haldane, *Phys. Rev. A* **2008**, *78*, 033834.
[267] B. Zhen, C. W. Hsu, Y. Igarashi, L. Lu, I. Kaminer, A. Pick, S.-L. Chua, J. D. Joannopoulos, M. Soljačić, *Nature* **2015**, *525*, 354.
[268] J. Mei, Y. Wu, C. T. Chan, Z.-Q. Zhang, *Phys. Rev. B* **2012**, *86*, 035141.
[269] Z. Lin, L. Christakis, Y. Li, E. Mazur, A. W. Rodriguez, M. Lončar, *Phys. Rev. B* **2018**, *97*, 081408.
[270] Z. Lin, A. Pick, M. Lončar, A. W. Rodriguez, *Phys. Rev. Lett.* **2016**, *117*, 107402.
[271] Y. Chen, F. Meng, G. Li, X. Huang, *Acta Mater.* **2019**, *164*, 377.
[272] R. V. Craster, S. Guenneau, in *Acoustic Metamaterials: Negative Refraction, Imaging, Lensing and Cloaking*, Springer Science+Business Media, Dordrecht, Netherlands **2013**.
[273] G. W. Milton, J. R. Willis, *Proc. R. Soc. A: Math. Phys. Eng. Sci.* **2007**, *463*, 855.
[274] Z. Liu, X. Zhang, Y. Mao, Y. Y. Zhu, Z. Yang, C. T. Chan, P. Sheng, *Science* **2000**, *289*, 1734.
[275] X. N. Liu, G. K. Hu, C. T. Sun, G. L. Huang, *J. Sound Vib.* **2011**, *330*, 2536.

© 2019 WILEY-VCH Verlag GmbH & Co. KGaA, Weinheim

25130390, 2019, 7, Downloaded from https://onlinelibrary.wiley.com/doi/10.1002/adts.201900017 by The Librarian, Wiley Online Library on [03/06/2024]. See the Terms and Conditions (https://onlinelibrary.wiley.com/terms-and-conditions) on Wiley Online Library for rules of use; OA articles are governed by the applicable Creative Commons License

[276] R. Zhu, X. N. Liu, G. K. Hu, C. T. Sun, G. L. Huang, *Nat. Commun.* **2014**, *5*, 5510.
[277] Z. Yang, J. Mei, M. Yang, N. H. Chan, P. Sheng, *Phys. Rev. Lett.* **2008**, *101*, 204301.
[278] H. H. Huang, C. T. Sun, *J. Acoust. Soc. Am.* **2012**, *132*, 2887.
[279] M. Yang, G. Ma, Z. Yang, P. Sheng, *Phys. Rev. Lett.* **2013**, *110*, 134301.
[280] T. Brunet, A. Merlin, B. Mascaro, K. Zimny, J. Leng, O. Poncelet, C. Aristégui, O. Mondain-Monval, *Nat. Mater.* **2015**, *14*, 384.
[281] J. H. Oh, Y. E. Kwon, H. J. Lee, Y. Y. Kim, *Sci. Rep.* **2016**, *6*, 23630.
[282] J. H. Oh, H. M. Seung, Y. Y. Kim, *Appl. Phys. Lett.* **2016**, *108*, 093501.
[283] J. Christensen, F. J. G. de Abajo, *Phys. Rev. Lett.* **2012**, *108*, 124301.
[284] V. M. García-Chocano, J. Christensen, J. Sánchez-Dehesa, *Phys. Rev. Lett.* **2014**, *112*, 144301.
[285] C. Shen, Y. Xie, N. Sui, W. Wang, S. A. Cummer, Y. Jing, *Phys. Rev. Lett.* **2015**, *115*, 254301.
[286] K. T. Tan, H. H. Huang, C. T. Sun, *Int. J. Impact Eng.* **2014**, *64*, 20.
[287] J. H. Oh, H. M. Seung, Y. Y. Kim, *J. Sound Vib.* **2017**, *410*, 169.
[288] W. M. Graeme, B. Marc, R. W. John, *New J. Phys.* **2006**, *8*, 248.
[289] H. Chen, C. T. Chan, *Appl. Phys. Lett.* **2007**, *91*, 183518.
[290] L. Zigoneanu, B.-I. Popa, S. A. Cummer, *Nat. Mater.* **2014**, *13*, 352.
[291] K. Muamer, B. Tiemo, S. Robert, W. Martin, *Rep. Prog. Phys.* **2013**, *76*, 126501.
[292] S. A. Cummer, J. Christensen, A. Alù, *Nat. Rev. Mater.* **2016**, *1*, 16001.
[293] D. Li, L. Zigoneanu, B.-I. Popa, S. A. Cummer, *J. Acoust. Soc. Am.* **2012**, *132*, 2823.
[294] L. Lu, T. Yamamoto, M. Otomori, T. Yamada, K. Izui, S. Nishiwaki, *Finite Elem. Anal. Des.* **2013**, *72*, 1.
[295] R. E. Christiansen, O. Sigmund, *Struct. Multidiscipl. Optim.* **2016**, *54*, 469.
[296] R. E. Christiansen, O. Sigmund, *Appl. Phys. Lett.* **2016**, *109*, 101905.
[297] H.-W. Dong, S.-D. Zhao, P. Wei, L. Cheng, C. Zhang, Y.-S. Wang, *Acta Mater.* **2018**. Available at SSRN: https://ssrn.com/abstract=3300933
[298] V. Fokin, M. Ambati, C. Sun, X. Zhang, *Phys. Rev. B* **2007**, *76*, 144302.
[299] H.-W. Dong, S.-D. Zhao, Y.-S. Wang, C. Zhang, *J. Mech. Phys. Solids* **2017**, *105*, 54.
[300] H.-W. Dong, S.-D. Zhao, Y.-S. Wang, C. Zhang, *Sci. Rep.* **2018**, *8*, 2247.
[301] J. Rong, W. Ye, *Comput. Methods Appl. Mech. Eng.* **2019**, *344*, 819.
[302] O. Sigmund, *Struct. Multidiscipl. Optim.* **2011**, *43*, 589.
[303] Z. Hashin, S. Shtrikman, *J. Mech. Phys. Solids* **1963**, *11*, 127.
[304] O. D. Miller, C. W. Hsu, M. T. H. Reid, W. Qiu, B. G. DeLacy, J. D. Joannopoulos, M. Soljačić, S. G. Johnson, *Phys. Rev. Lett.* **2014**, *112*, 123903.
[305] O. D. Miller, A. G. Polimeridis, M. T. Homer Reid, C. W. Hsu, B. G. DeLacy, J. D. Joannopoulos, M. Soljačić, S. G. Johnson, *Opt. Express* **2016**, *24*, 3329.

© 2019 WILEY-VCH Verlag GmbH & Co. KGaA, Weinheim

25130390, 2019, 7, Downloaded from https://onlinelibrary.wiley.com/doi/10.1002/adts.201900017 by The Librarian, Wiley Online Library on [03/06/2024]. See the Terms and Conditions (https://onlinelibrary.wiley.com/terms-and-conditions) on Wiley Online Library for rules of use; OA articles are governed by the applicable Creative Commons License